

# Water Resources Research®



## RESEARCH ARTICLE

10.1029/2023WR034621

## Stiff, Smooth, and Solid? Complex Fracture Hydraulics' Imprint on Oscillatory Hydraulic Testing

Jeremy R. Patterson<sup>1,2</sup>  and Michael Cardiff<sup>1</sup> 

<sup>1</sup>Department of Geoscience, University of Wisconsin-Madison, Madison, WI, USA, <sup>2</sup>Earth, Environmental, and Planetary Science, Rice University, Houston, TX, USA

### Key Points:

- Heterogeneous fracture storage, fracture-host rock fluid exchange, and hydromechanics all produce period-dependent effective parameters
- Each explored mechanism produces distinct—potentially diagnostic—period-dependent hydraulic parameter estimates
- Fracture hydromechanics is the only mechanism that reproduces period-dependent parameter trends described in previous field experiments

### Supporting Information:

Supporting Information may be found in the online version of this article.

### Correspondence to:

J. R. Patterson,  
jp128@rice.edu

### Citation:

Patterson, J. R., & Cardiff, M. (2023). Stiff, smooth, and solid? Complex fracture hydraulics' imprint on oscillatory hydraulic testing. *Water Resources Research*, 59, e2023WR034621. <https://doi.org/10.1029/2023WR034621>

Received 10 FEB 2023  
Accepted 1 NOV 2023

### Author Contributions:

**Conceptualization:** Jeremy R. Patterson, Michael Cardiff  
**Formal analysis:** Jeremy R. Patterson  
**Funding acquisition:** Michael Cardiff  
**Investigation:** Jeremy R. Patterson  
**Methodology:** Jeremy R. Patterson  
**Project Administration:** Michael Cardiff  
**Software:** Michael Cardiff  
**Supervision:** Michael Cardiff  
**Validation:** Jeremy R. Patterson  
**Visualization:** Jeremy R. Patterson  
**Writing – original draft:** Jeremy R. Patterson

© 2023 The Authors.

This is an open access article under the terms of the [Creative Commons Attribution-NonCommercial License](https://creativecommons.org/licenses/by-nc/4.0/), which permits use, distribution and reproduction in any medium, provided the original work is properly cited and is not used for commercial purposes.

**Abstract** Fractured bedrock aquifers, especially deep aquifers, represent increasingly common targets for waste storage and alternative energy development, necessitating detailed quantitative descriptions of fracture hydraulic properties, geometry, and connectivity. Yet, multi-scale characterization of the physical properties that govern fluid flow through and storage in fractured bedrock remains a fundamental hydrogeologic challenge. Oscillatory hydraulic testing, a novel hydraulic characterization technique, has been showing promise in field experiments to characterize the effective hydraulic properties of bedrock fractures. To date, these characterization efforts utilize simplified diffusive analytical models that conceptualize a non-deforming, parallel-plate fracture embedded within impermeable host rock, and have found that the returned fracture hydraulic parameter estimates exhibit an apparent period-dependence. We conduct synthetic experiments using three different numerical models to examine proposed mechanisms that might contribute to the observed period-dependence including heterogeneous flow and storage within the fracture (i.e., aperture heterogeneity), fracture-host rock fluid exchange, and fracture hydromechanics. This work represents the first systematic analysis that seeks to understand the process(es) occurring within a bedrock fracture that might be contributing to this apparent period-dependence. Our analysis demonstrates that all investigated mechanisms generate period-dependent effective hydraulic parameter estimates, each with their own potentially diagnostic trends; however, fracture hydromechanics is the only explored mechanism that consistently reproduces period-dependent trends in parameter estimates that are consistent with existing field investigations. These results highlight the need to develop more complex numerical modeling approaches that account for this hydromechanical behavior when characterizing fractured bedrock aquifers.

**Plain Language Summary** Deep aquifers frequently contain multiple fractures that provide channels for rapid transport and storage of water, heat, and contaminants through the subsurface, making them increasingly popular resources for alternative energy and waste storage. Building computer models that create accurate predictive simulations of flow and transport through fractured bedrock requires detailed knowledge and description of the physical properties that govern flow and transport through and the hydraulic processes occurring within these fractures. Periodic pressure testing has recently been used to determine these hydraulic properties; however, they have been found to be dependent on the period of the pressure signal, which indicates the presence of hydraulic processes occurring within the fracture that are not considered during analysis. We use three computer models to investigate potential mechanisms that might contribute to this apparent period-dependence, and we find that fracture displacement due to pressure changes along the fracture leads to inaccurate averaged fracture flow parameter estimates when simple analytical expressions are used during data analysis.

## 1. Introduction

Fractured bedrock aquifers—where fractures provide the primary conduits for fluid flow and pressure propagation—represent an important and increasingly utilized resource for geothermal heat extraction (Fu et al., 2016; McClure & Horne, 2014; Wu et al., 2021), geologic carbon sequestration (Fu et al., 2017; A. Y. Sun et al., 2015; Y. Sun & Tong, 2017), and nuclear waste storage (Cuss et al., 2015; Tsang et al., 2015). Accurate multi-scale prediction of fluid flow pathways through fractured bedrock systems is necessary for successful adoption of the above alternative energy and waste injection strategies. Yet, these accurate predictive simulations often remain elusive due to the complex three-dimensional flow occurring in these systems (National Academies of Sciences, Engineering, and Medicine, 2020).

Writing – review & editing: Jeremy R. Patterson, Michael Cardiff

Characterizing the hydraulic properties, geometry, and connectivity of bedrock fractures remains a fundamental hydrogeologic challenge (Becker et al., 2020; Berre et al., 2019; Bonnet et al., 2001). Though geophysical and tracer methods are commonly used to quantify fracture flow and transport properties as well as fracture connectivity (e.g., Becker & Tsoflias, 2010; Klepikova et al., 2014; Roubinet et al., 2016; Talley et al., 2005), pressure-based characterization methods—where a pressure stimulus is introduced at a point and the response is measured at surrounding locations—provide the most direct local information on the hydraulic properties that govern flow and storage within an individual fracture (Cardiff et al., 2012). Historically, the single-well slug test and cross-well constant-rate pumping test—which hydraulically stress fractured bedrock at significantly different scales—represent the most commonly applied pressure-based characterization approaches due to minimal equipment requirements and relative ease of implementation (Butler Jr, 2005).

Oscillatory hydraulic testing—where water is alternatively injected into and pumped from a well in a periodic manner—represents an alternative hydraulic characterization approach designed to “bridge the gap” between pumping tests and slug tests that has multiple advantages over traditional pressure-based characterization methods. Oscillatory hydraulic tests are capable of testing fractures across multiple scales by simply changing the frequency at which pumping and injection are alternated, allowing investigators to tune the scale of hydraulic testing to their desired area of interest (Cardiff et al., 2013). In contrast to constant-rate pumping tests, oscillatory hydraulic tests can be designed in a mass-conservative manner such that there is no net water extraction or injection into tested fractures, thereby minimizing alterations to the ambient stress and flow fields along the fracture (Cardiff & Barrash, 2015; Rabinovich et al., 2015). In applications that require continuous pumping (e.g., geothermal production), a periodic pressure signal can be superimposed at the pumping well by systematically varying flow rates above and below a long-term pumping rate, allowing reservoir characterization to occur without interrupting production operations and minimizing revenue losses (Fischer et al., 2018; Fokker et al., 2021; Salina Borello et al., 2019). Finally, because the frequency of the input signal is known, recorded observation signals are readily extracted from instrument noise, instrument drift, and/or hydrologic noise (e.g., evapotranspiration and recharge events) using standard linear signal processing techniques (Bakhos et al., 2014).

Multiple studies illustrate the utility of natural and introduced periodic pressure signals to characterize hydraulic properties in alluvial aquifers (Ferris, 1952; Rabinovich et al., 2015; Sobolevskaia et al., 2021), unconsolidated sedimentary aquifers (Rasmussen et al., 2003), and petroleum reservoirs (Hollaender et al., 2002; Johnson et al., 1966; Kuo, 1972). Renner and Messar (2006) conducted a series of periodic pumping tests with oscillation periods across more than two orders-of-magnitude, representing one of the earliest applications of periodic pumping tests to characterize fractured bedrock. Follow-on studies demonstrated that periodic pressure signals can be used to infer fracture connectivity (Becker & Gultinan, 2010; Gultinan & Becker, 2015) and flow geometry in complex fracture networks (Sayler et al., 2018). More recently, Patterson and Cardiff (2023) presented the first known application of oscillatory hydraulic testing in an isolated fracture embedded in high-permeability sedimentary bedrock and demonstrated fluid exchange occurring between the tested fracture and surrounding host rock during their field experiments.

Following a long history of effective parameter estimation approaches to characterize subsurface hydraulic properties, previous field experiments (Gultinan & Becker, 2015; Patterson & Cardiff, 2023; Renner & Messar, 2006; Sayler et al., 2018) applied simple “stiff, smooth, and solid” diffusive analytical models which relate amplitude attenuation and phase delay to effective fracture hydraulic properties (Black & Kipp, 1981; Rasmussen et al., 2003). Under the assumption that the tested fracture can be described as a non-deforming fracture with homogenous and isotropic flow properties bounded by impermeable host rock, these field studies reveal a repeatable apparent period-dependence in effective fracture hydraulic parameter estimates. Specifically, these studies reported decreasing hydraulic diffusivity estimates with increasing oscillation period, which is driven by storativity estimates that increase with increasing oscillation period (Gultinan & Becker, 2015; Patterson & Cardiff, 2023; Renner & Messar, 2006; Sayler et al., 2018). Previously unreported in the literature, Patterson and Cardiff (2023) also found spatial trends in effective parameter estimates with increasing diffusivity and decreasing storativity estimates with increasing inter-well spacing for a given oscillation period, which provides another indication that the inherent assumptions of simple diffusive models are not met in fractured bedrock settings.

The repeatable apparent period-dependence in effective fracture hydraulic parameter estimates reported across multiple studies indicates that conceptualizing fractures as non-deforming, smooth surfaces bounded by impermeable rock—that is, the traditional “parallel-plate” model—does not adequately capture the complex hydraulics

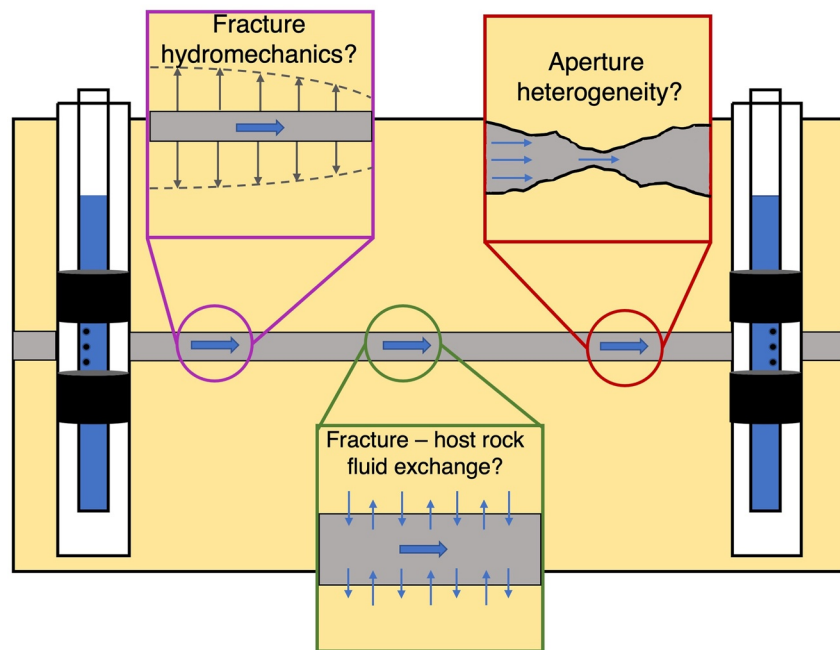


**Figure 1.** Conceptual diagram showing potential flow processes occurring within an individual fracture—and explored through detailed numerical modeling—that potentially contribute to the apparent period-dependence in effective fracture hydraulic parameter estimates.

occurring in fractured rock during oscillatory hydraulic testing. Renner and Messar (2006) proposed that the apparent period-dependence results from fluids interacting with flow-restricted areas of fractures (i.e., fracture asperities) that do not significantly contribute to flow at the longest oscillation periods. Another way to conceptualize this hypothesis in a more general sense is that high-permeability flow channels (i.e., a “backbone”) along the fracture are bounded by low-permeability regions of fluid storage that do not contribute to flow—either through dead-end pore space within the fracture or fluid exchange between the fracture and surrounding host-rock—and fluid residence time within the fracture increases as the oscillation period increases, allowing more time for fluid diffusion into these flow restricted regions.

Alternatively, Guiltinan and Becker (2015) posit that the apparent period-dependence results from normal displacement of fracture surfaces in response to pressure changes along the fracture during hydraulic testing (i.e., fracture hydromechanical behavior). This hypothesis is supported by a long history of field experiments that have measured this fracture hydromechanical response during slug testing and constant-rate pumping tests (Cappa et al., 2005, 2006; Schweisinger et al., 2009, 2011; Svenson et al., 2007, 2008) as well as oscillatory hydraulic tests with head change amplitudes down to the mm-scale (Becker et al., 2017), yet remains untested.

Field experimental setups may also inadvertently lead to an apparent period-dependence in returned hydraulic parameter estimates. For example, non-Darcian flow or borehole storage effects on test analysis may lead to errors in test interpretation (e.g., Quinn et al., 2011; Xing et al., 2022). Patterson and Cardiff (2023) used simple analyses and analytical models to explore the potential of non-Darcian flow and borehole storage as potential mechanisms contributing to the period-dependent flow parameters returned during their field experiments and showed that these experimental design effects do not fully account for the apparent period-dependence in effective hydraulic parameter estimates.

Despite multiple working hypotheses, the hydraulic and/or hydromechanical processes that might be contributing to the apparent period-dependent effective fracture hydraulic parameters remain an open question. In this analysis, we present a numerical modeling study that systematically explores three candidate processes occurring in fractured bedrock (Figure 1)—heterogeneous flow and storage, fracture-host rock fluid exchange, and fracture hydromechanics—that have been proposed to contribute to the repeatable period-dependent trend in effective hydraulic parameter estimates. This study uses multiple numerical models representing each candidate process—

**Table 1**  
*Well Coordinates for Numerical Modeling Simulations*

Well name	X location (m)	Y location (m)
A1	0	0
B1	0	10
B2	8	0
B3	0	-4
B4	-6	0

alone and together—to generate oscillatory hydraulic data, and then follows the analysis approach of previous fracture characterization studies by relating the amplitude attenuation and phase delay—output by our numerical models—to effective fracture hydraulic parameters using a simplified “stiff, smooth, and solid” diffusive analytical model (Sections 3.1–3.3).

Finally, we investigate which candidate mechanism reproduces the repeatable period-dependent parameter estimates reported in the literature (Section 3.4). To demonstrate the utility of these potentially diagnostic period-dependent parameter trends, we present the fracture characterization results from Patterson and Cardiff (2023)—which are representative of the period-dependent trends reported throughout the literature—as a baseline for

comparison against our numerical modeling analyses. The interested reader will find a brief site description for the referenced field study in Supporting Information S1. However, the focus of our current work is on understanding how fundamental hydraulic processes occurring within a fracture during oscillatory hydraulic testing affect the obtained “effective” hydraulic parameter results, rather than generating site-specific characterization results. For this reason, we opt to use more generalized numerical modeling approaches as opposed to including the geometric and hydraulic complexities of site-specific models.

## 2. Modeling Approaches

We developed three numerical models that each represent a hydraulic process hypothesized to contribute to the apparent period-dependence in effective fracture hydraulic parameter estimates (Figure 1). Specifically, we developed a 2-D phase-domain hydraulic model to explore the effects of heterogeneous flow and storage within the fracture, a 3-D phase-domain hydraulic model to investigate the effects of fracture-host rock fluid exchange, and a time-domain hybrid-dimensional hydromechanical model that explores the effects of the fracture hydro-mechanical response on recorded observation signals and the returned effective fracture hydraulic parameter estimates. We applied the developed models to understand how these mechanisms—acting alone and together—might contribute to apparent period-dependent trends in effective hydraulic parameters.

The developed models simulate oscillatory hydraulic tests with oscillation periods from 10 to 1,000 s, chosen to be consistent with the range of oscillation periods used in previous field experiments (Becker & Gultinan, 2010; Gultinan & Becker, 2015; Patterson & Cardiff, 2023; Renner & Messar, 2006). Each simulated oscillatory hydraulic test generates a pumping signal at one well, while recording the resulting pressure signals at four observation wells. We simulated these oscillatory tests within a “5-spot” well arrangement as described in Table 1, and took a tomographic approach to our test design by rotating the pumping location across all wells—generating all possible source-receiver combinations without repetition—which creates inter-well spacings from 4 to 16 m, consistent with well spacings used in previous field experiments. The amplitude of the pumping signal during oscillatory hydraulic testing can be controlled by constraining the total volume cycled during one oscillation period or by constraining the peak volumetric flow rate. We apply a constant peak volumetric flow rate across all oscillation periods to control the amplitude of the pumping signal. Finally, we repeated the analysis approach of previous studies—described in detail in Section 2.4—by inverting each individual observation signal to obtain effective hydraulic parameters; each oscillatory hydraulic test thus produces four sets of effective parameter estimates, associated with the four individual observation signals.

For the purposes of this work, we assume the observation signal is recorded with no instrument noise, which allows us to isolate the impact of hydraulic processes on effective parameter estimates without the added complications of data quality control and signal extraction from instrument noise and/or drift. Our approach of recording pressure responses at variable oscillation periods and multiple inter-well spacings allows us to assess not only the apparent period-dependence, but also spatial trends in parameter estimates returned through inverse modeling.

### 2.1. Heterogeneous Flow and Storage

We developed a square (2D) model—with model dimensions given in Table 2—that approximates flow through a semi-infinite, non-deforming, variable-aperture fracture embedded in impermeable host rock to explore the effects of heterogeneous flow and storage within the fracture on effective hydraulic parameter estimates. The

**Table 2**  
*Heterogeneous Fracture Modeling Parameters*

Parameter	Value
Model geometry	
Domain size	3,000 m × 3,000 m
Grid discretization ( $\Delta x, \Delta y$ )	2 m
Geostatistical parameters	
Mean aperture ( $b$ )	0.3 mm
Variance $\ln(b)$	0.3
X correlation length	20 m
Y correlation length	5 m
Fracture hydraulic properties	
Peak flow rate ( $Q_0$ )	$7 \times 10^{-5} \text{ m}^3/\text{s}$
Mean transmissivity ( $\overline{T_f}$ )	$2.2 \times 10^{-5} \text{ m}^2/\text{s}$
Mean storativity ( $\overline{S_f}$ )	$2.6 \times 10^{-8}$
Mean hydraulic diffusivity ( $\overline{D_f}$ )	$846 \text{ m}^2/\text{s}$

model simulates flow through the fracture using the steady-periodic formulation of the confined groundwater flow equation (Cardiff et al., 2013) with prescribed head amplitude boundaries on all sides and no-flow boundaries on the model top and bottom:

$$i\omega S_f \Phi = \nabla \cdot (T_f \nabla \Phi) + Q_\omega \quad \forall \mathbf{x} \in \Omega \quad (1)$$

$$\Phi = 0 \quad \forall \mathbf{x} \in \Gamma_d \quad (2)$$

$$\nabla \cdot \mathbf{n} = 0 \quad \forall \mathbf{x} \in \Gamma_n \quad (3)$$

where  $\Phi [L]$  is the complex-valued head phasor for pumping frequency  $\omega = 2\pi/P [1/T]$ ,  $T_f [L/T^2]$  is the fracture transmissivity,  $S_f [-]$  is fracture storativity,  $Q_\omega [1/T]$  is the pumping signal phasor,  $i$  is the imaginary number  $\sqrt{-1}$ ,  $\Omega$  is the modeling domain,  $\Gamma_d, \Gamma_n$  are Dirichlet and Neumann boundary conditions, respectively, and  $\mathbf{n}$  is the outward normal for the given boundaries. The simulated head and pumping phasors can be translated to head changes and pumping rates in the time domain as:

$$h(\mathbf{x}, t) = \text{Re}[\Phi(\mathbf{x})\exp(i\omega t)] \quad (4)$$

$$q(\mathbf{x}, t) = \text{Re}[Q_\omega(\mathbf{x})\exp(i\omega t)] \quad (5)$$

We used OHT3DINV (Cardiff, 2016)—an open-source, MATLAB-based steady-periodic numerical forward model—to solve the boundary value problem given by Equations 1–3 using a finite volume approach. This analysis assumes that any initial transients have dissipated and flow through the fracture can be modeled by simulating the spatially varying, but temporally invariant head phasor (Cardiff et al., 2013).

To provide the hydraulic input parameters for OHT3D, we converted spatially correlated aperture realizations to transmissivity ( $T$ ), assuming the local cubic law (Zimmerman & Bodvarsson, 1996) is valid at each discrete point in the fracture plane as follows:

$$T_f(\mathbf{x}) = \frac{\gamma_f b(\mathbf{x})^3}{12\mu_f} \quad (6)$$

This model uses the standard linear elastic groundwater storage equation to represent fracture storativity. Under the simplifying assumption of non-deformable fracture walls that do not touch at any point (i.e.,  $\eta = 1$ ), storativity is a function of fluid compressibility and can be calculated as follows:

$$S_f(\mathbf{x}) = \gamma_f \eta \beta_f b(\mathbf{x}) \quad (7)$$

where  $\mathbf{x} = [x, y]$  is a vector of spatial coordinates,  $\gamma_f = \rho_f g [M/(L^2 T^2)]$  is the specific weight of the fluid,  $\rho_f [M/L^3]$  is the fluid density,  $g [L/T^2]$  is gravitational acceleration,  $\mu_f [M/(LT)]$  is the fluid dynamic viscosity,  $\eta [-]$  is porosity, and  $\beta_f [(LT^2)/M]$  is fluid compressibility.

To verify model accuracy and ensure hydraulic boundaries do not affect the solution within the area of interest, we compare numerically simulated head phasors at the observation wells in a homogeneous fracture plane—using the mean aperture (Table 2)—to simulated head phasors given by the steady-periodic analytical model for a fully confined homogeneous aquifer as presented by Rasmussen et al. (2003). Across all oscillation periods, the numerically simulated head amplitudes matched the analytical head amplitudes by 1 mm or less. This level of numerical modeling error cannot be differentiated from data measurement error based on current pressure sensor technology (Leven & Barrash, 2022; Patterson & Cardiff, 2022).

We generated two heterogeneous aperture realizations using an exponential variogram model with the geostatistical parameters given in Table 2. These realizations represent two end-member aperture distributions: (a) the central well located in a highly transmissive (i.e., larger aperture) region surrounded by flow-restricted regions (i.e., smaller aperture regions) (Figure 2a) and (b) the central well located in a flow restricted region surrounded by highly transmissive areas (Figure 2c). The chosen geostatistical parameters generate highly anisotropic aperture

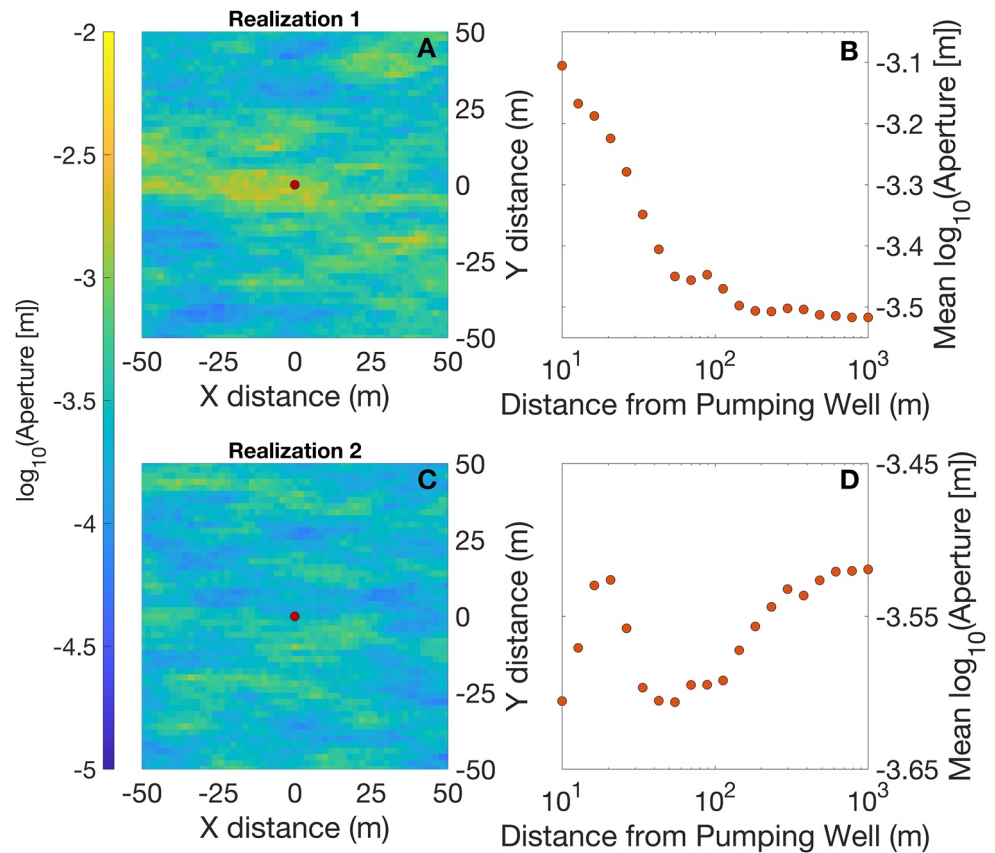


**Figure 2.** Heterogeneous aperture realizations used to explore the effects of heterogeneous flow and storage on effective hydraulic parameter estimates. (a) and (c) Show aperture geostatistical aperture realizations with the red circle indicating the central pumping well (A1). Surrounding observation wells are omitted for clarity. (b) and (d) Show the geometric mean of the hydraulic radius for a given oscillation period.

**Table 3**  
Fracture-Host Rock Fluid Exchange Modeling Parameters

Parameter	Value
Model geometry	
Domain size	800 m × 800 m × 0.65 m
Horizontal discretization ( $\Delta x, \Delta y$ )	2 m
Vertical discretization ( $\Delta z$ )	0.05 m
Fracture hydraulic properties	
Peak flow rate ( $Q_0$ )	$7 \times 10^{-5}$ m <sup>3</sup> /s
Fracture hydraulic conductivity ( $K_f$ )	$2.2 \times 10^{-4}$ m/s
Fracture-specific storage ( $S_{if}$ )	$2.6 \times 10^{-7}$ m <sup>-1</sup>
Fracture hydraulic diffusivity ( $D_f$ )	846 m <sup>2</sup> /s
Host rock hydraulic properties	
Host rock porosity ( $\eta$ )	0.15 (-)
Host rock hydraulic conductivity ( $K_r$ )	$3.0 \times 10^{-8}$ m/s
Host rock-specific storage ( $S_{sr}$ )	$1.4 \times 10^{-4}$ m <sup>-1</sup>
Host rock hydraulic diffusivity ( $D_r$ )	$2.1 \times 10^{-4}$ m <sup>2</sup> /s

fields with large-scale spatially correlated structures that span the area of interest (i.e., the well-field), consistent with lab-scale aperture distribution analyses (Auradou et al., 2006; Drazer et al., 2004). The chosen aperture mean and variance (Table 2) are motivated by field-scale effective hydraulic aperture estimates (Patterson & Cardiff, 2023) and core-scale aperture distribution analyses (Hakami & Larsson, 1996).

## 2.2. Fracture-Host Rock Fluid Exchange

Fractures embedded in permeable host rock—such as fractured sandstone aquifers—represent an added level of complexity with the presence of fast flow paths along the fracture, slower porous-media dominated flow paths, and fracture-host rock fluid exchange occurring along pressure gradients, which has been demonstrated in low-permeability (Neretnieks, 2006) and high-permeability bedrock settings (Patterson & Cardiff, 2023).

We developed a large rectangular prism model—with dimensions given in Table 3—that approximates flow through a semi-infinite, non-deforming fracture bounded by a permeable host rock to explore the effects of these fracture-host rock hydraulic interactions on estimated effective fracture hydraulic parameters. This model represents the top half of a flat-lying fracture bounded by high-permeability host rock (Figure 3). We placed wells at the center of the model fracture layer (Figure 3) using the horizontal coordinates

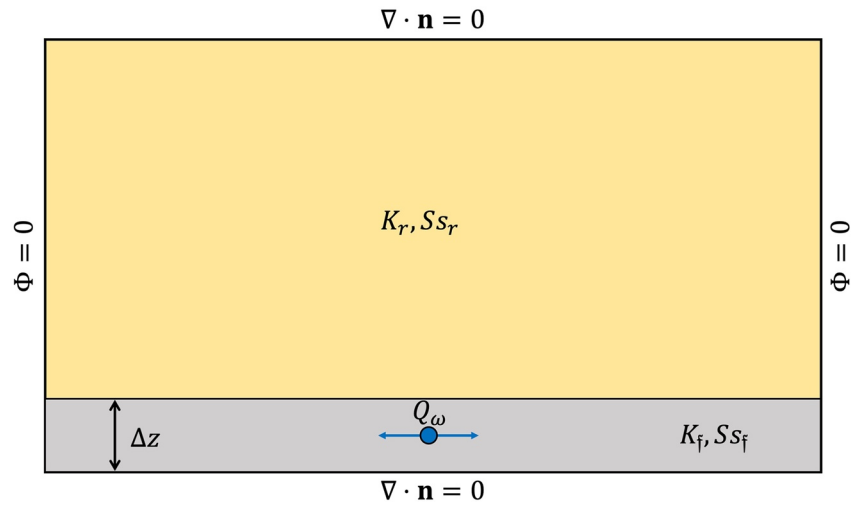


**Figure 3.** Conceptual vertical slice through the 3-D modeling domain showing the top half of a symmetric, parallel-plate half-fracture (gray rectangle) embedded in a permeable host rock (tan rectangle). The blue circle shows the location of Well A1 (Table 1) within the fracture. Remaining wells are excluded for clarity.

provided in Table 1. The model simulates flow through the fractured aquifer using the steady-periodic formulation of the groundwater flow equation with prescribed head amplitude at the lateral boundaries and no-flow boundaries applied to the model top and bottom:

$$i\omega S_s \Phi = \nabla \cdot (K \nabla \Phi) + Q_\omega \quad \forall \mathbf{x} \in \Omega \quad (8)$$

$$\Phi = 0 \quad \forall \mathbf{x} \in \Gamma_d \quad (9)$$

$$\nabla \cdot \mathbf{n} = 0 \quad \forall \mathbf{x} \in \Gamma_n \quad (10)$$

OHT3DINV solves the boundary value problem given by Equations 8–10 and simulates the steady-periodic head phasors throughout the modeling domain using the hydraulic parameters given in Table 3. We compare modeled phasors at observation wells with the analytical model for a leaky confined aquifer developed by Rasmussen et al. (2003) to verify model accuracy and ensure modeled phasors are not impacted by hydraulic boundaries. Across all oscillation periods, the numerically simulated head amplitudes matched the analytical head amplitudes within 1 mm or less. This level of numerical modeling error cannot be differentiated from data measurement error of commonly employed head change sensors (Leven & Barrash, 2022; Patterson & Cardiff, 2022).

We applied the developed model to two scenarios: (a) the isolated effect of fracture-host rock fluid exchange and (b) the combined effects of fracture-host rock fluid exchange and aperture heterogeneity on effective hydraulic parameter estimates. First, we considered the isolated effects of fracture-host rock fluid exchange with a smooth-walled fracture. We prescribed homogeneous fracture hydraulic conductivity and specific storage values that maintain a consistent characteristic diffusion length through the fracture across this model and the 2-D model described in Section 2.1. To achieve this, we used the prescribed mean transmissivity and storativity values given in Table 2 to calculate the fracture hydraulic conductivity and specific storage as follows:

$$K_f = \frac{\overline{T}_f}{2\Delta z} \quad (11)$$

$$S_{s_f} = \frac{\overline{S}_f}{2\Delta z} \quad (12)$$

where  $K_f$  [L/T] is the fracture hydraulic conductivity,  $S_{s_f}$  [1/L] is the fracture-specific storage applied, and  $\Delta z$  is the vertical discretization [L]. The  $2\Delta z$  factor in Equations 11 and 12 arises from the fact that the model bottom is a symmetry boundary, and thus represents a fracture half-aperture. We prescribed homogeneous host rock hydraulic parameters representative of highly permeable, mature sandstone units, such as the Mt. Simon

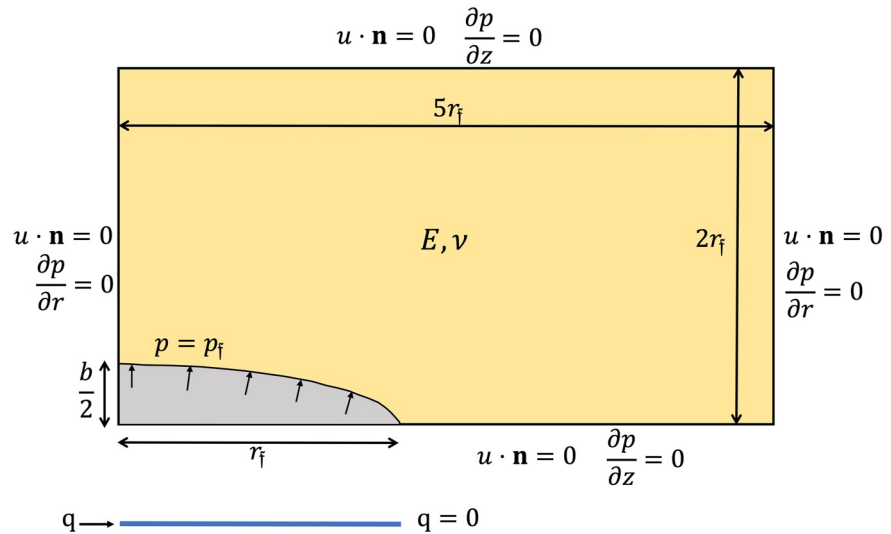


**Figure 4.** Conceptual sketch of the hybrid-dimensional hydromechanical model. The rectangle represents the 2-D axisymmetric mechanical modeling domain, with the blue arc representing the top half of a symmetric fracture as a high aspect ratio ellipse. The left and bottom model boundaries represent symmetry planes. The solid blue line represents the 1-D axisymmetric hydraulic modeling domain.

Formation, which serves as a major municipal water source (Gellasch et al., 2013, 2014) and is actively being investigated as a site for potential geologic carbon sequestration (Luu et al., 2022).

For the second modeling scenario, we loosened the assumption of a smooth-walled fracture to explore the combined impacts of fracture host-rock fluid exchange and heterogeneous flow and storage within the fracture on effective hydraulic parameter estimates. We used the geostatistical parameters given in Table 2 to generate heterogeneous aperture fields consistent with Realizations 1 and 2 (Figure 2) and converted those aperture fields to fracture hydraulic conductivity and specific storage using Equations 11 and 12. For this modeling scenario, we maintained the assumption of homogeneous hydraulic parameters in the surrounding host rock (Table 3).

### 2.3. Fracture Hydromechanics

Models simulating subsurface flow and storage through bedrock fractures frequently represent the fracture as a non-deforming solid despite recent field experiments (e.g., Becker et al., 2017; Dutler et al., 2020; Schweisinger et al., 2011) and modeling studies (Schmidt et al., 2021; Vinci et al., 2015) demonstrating the importance of the hydromechanical coupling in fractured bedrock settings. To explore the effects of hydromechanical behavior during oscillatory hydraulic testing on effective hydraulic parameter estimates, we used the hybrid-dimensional hydromechanical model developed by Vinci et al. (2014), which consists of a coupled 1-D hydraulic model and a 2-D linear elastic model to simulate flow through and the displacement of a deformable, semi-infinite fracture. The model represents the top half of a radially symmetric, flat-lying fracture embedded in low-permeability bedrock (Figure 4).

Our choice to employ a model that assumes a fully open, parallel-plate fracture has limitations with respect to the role of asperities in the hydromechanical response during hydraulic testing. Our model relates fracture stiffness to deformation sensitivity to fluid pressure changes along the entire fracture, which is only true in mechanically open portions of natural rock fractures. In regions of the fracture where fracture surfaces are in contact, fracture stiffness is related to the elastic moduli of the host rock, enhancing the apparent fracture stiffness (Murdoch & Germanovich, 2006; Vinci et al., 2015). While more sophisticated modeling approaches exist that account for the impact of asperities on fracture stiffness (e.g., Murdoch & Germanovich, 2006), we opted for a modeling approach with the least complexity that allows us to investigate the impact of the fracture hydromechanical response on effective fracture hydraulic parameter estimates. This modeling decision likely underestimates fracture stiffness—and thus overestimates the hydromechanical response—which is critical for site-specific characterization efforts. However, our approach is sufficient to investigate whether

fracture hydromechanics is a hydraulic process occurring in bedrock fractures that can reproduce the apparent period-dependence in effective hydraulic parameter estimates. To address the limitations of a fully open fracture, we attempted to mimic the enhanced fracture stiffness due to asperities by prescribing artificially inflated elastic moduli to the surrounding rock, with a drained bulk modulus that is consistent with apparent fracture stiffness values reported during hydromechanical well testing (Becker et al., 2017; Schweisinger et al., 2009; Svenson et al., 2008).

The hydraulic model simulates fluid flow along the fracture as a 1-D axisymmetric process (Figure 4) using the governing equation for flow through a deformable fracture derived by Vinci et al. (2014) starting from basic mass and momentum conservation:

$$\frac{\partial p}{\partial t} + \frac{1}{12\mu_f r} \frac{\partial}{\partial r} \left( -\frac{rb^2}{\beta_f} \frac{\partial p}{\partial r} \right) - \frac{1}{12\mu_f} \left( \frac{b}{\beta_f} \frac{\partial b}{\partial r} \right) \frac{\partial p}{\partial r} - \frac{b^2}{12\mu_f} \left( \frac{\partial p}{\partial r} \right)^2 = -\frac{1}{\beta_f b} \frac{\partial b}{\partial t} + q_l \quad (13)$$

This governing equation contains—presented from left to right—a transient pressure term, a diffusion term, a convection term, a quadratic term, a solid displacement coupling term, and a source term that allows fluid leakage from the fracture assuming Darcian flow in the surrounding host rock. The interested reader is directed to Vinci et al. (2014) for further details.

For the hydraulic model, we prescribe a fracture radius ( $r_f$ ) of 150 m with a no-flow boundary condition applied at the fracture tip and a specified-flux boundary condition at the borehole wall ( $r_w$ ) given by:

$$v_f(r_w, t) = \frac{q(t)}{2\pi r_w b(r_w, t)} \quad (14)$$

where  $v_f [L/T]$  is the fluid velocity along the fracture and  $q [L^3/T]$  is the oscillatory pumping signal given by:

$$q(t) = Q_0 \left[ 1 - \exp\left(-\frac{t}{t_s}\right) \right] \sin\left[(t + [t_{off} P])\omega\right] \quad (15)$$

where  $P [T]$  is the prescribed oscillation period,  $t [T]$  is time,  $t_s [T]$  is the pumping ramp-up time—set to the prescribed period of oscillation—and  $t_{off} [-]$  is time offset relative to a sine wave. This oscillatory pressure signal contains a period of initial transience that ramps up to a steady-periodic signal with the pumping amplitude prescribed by the peak volumetric flow rate ( $Q_0$ ).

The mechanical model simulates fracture normal displacement as a 2-D axisymmetric process (Figure 4) assuming an isotropic linear elastic material with Young's modulus ( $E$ ) and Poisson's ratio ( $\nu$ ) describing the stiffness of the mechanical domain. We represent the fracture in the mechanical domain as a high-aspect-ratio ellipse, with the major axis representing the fracture radius ( $r_f$ ) and the minor axis representing the fracture half-aperture ( $b/2$ ) (Figure 4). The mechanical domain is 750 m in length and 300 m in height, avoiding far-field boundary effects on the fracture normal displacement response in the area of interest. We place observation wells every 2 m along the fracture wall from 4 to 16 m, which is consistent with the inter-well spacings in Sections 2.1 and 2.2.

We applied a specified pressure boundary to the fracture wall—passed from the hydraulic model—to maintain pressure equilibrium between the hydraulic and mechanical models (Figure 4). Fluid pressure changes along the fracture result in normal displacement of the fracture wall, which couples to the aperture in the hydraulic model (Equation 13). For the purposes of this work, negative displacement represents compression. We specify lateral model boundaries as roller boundaries, with the model left and bottom boundaries representing planes of symmetry (Figure 4). We use COMSOL Multiphysics 5.6 to solve the hydraulic and mechanical problems in an iteratively coupled manner, with the fracture aperture representing the coupling variable.

The hydromechanical model outputs a time series of head and normal displacement at observation wells along the fracture, with the mechanical response preceding the hydraulic response at the observation wells (Figure 5). Both signals exhibit an initial transience of three oscillation periods before arriving at a steady-periodic (i.e., constant amplitude and phase) state (Figure 5). The steady-periodic portion of the signals can be described by the real component of a complex exponential function as follows:

$$\mathbf{h}(r, t) = \text{Re}[\Phi \exp(i\omega t)] \quad (16)$$

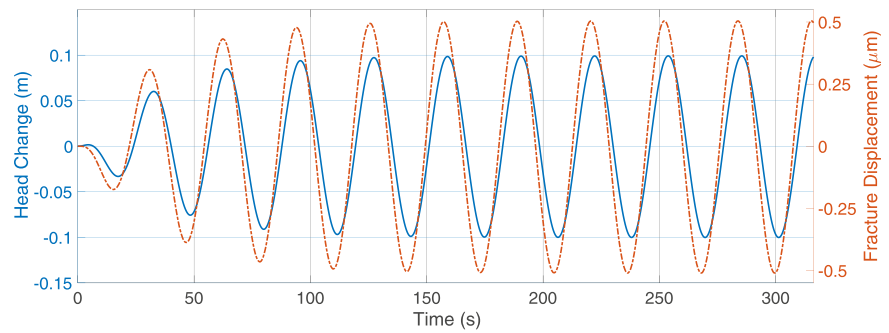


**Figure 5.** Representative pressure and fracture displacement time series for an oscillatory hydraulic test with a 30-s oscillation period at a radial distance of 10 m from the oscillation well. The solid blue line (left axis) shows the head change signal, and the dashed orange line (right axis) represents the fracture displacement signal, with the mechanical signal preceding the pressure signal. Both signals achieve a steady-periodic state after three full oscillation periods.

To extract the head phasors used during inverse modeling, we apply Euler's formula and represent Equation 16 as a linear combination of sinusoids as follows (Bakhos et al., 2014; Cardiff & Saylor, 2016):

$$\mathbf{h}(r, t) = \Phi_r \cos(\omega t) - \Phi_i \sin(\omega t) \quad (17)$$

Leveraging the linearity of Equation 17, we can write the system of equations in matrix form and use standard linear regression to extract the head phasor following Bakhos et al. (2014). The extracted head phasor provides the simulated data used to estimate the fracture hydraulic parameters as described in Section 2.4.

$$\mathbf{h} = \mathbf{X}\Phi, \mathbf{X} = \begin{bmatrix} \cos(\omega t_1) & -\sin(\omega t_1) \\ \vdots & \vdots \\ \cos(\omega t_n) & -\sin(\omega t_n) \end{bmatrix}, \Phi = \begin{bmatrix} \Phi_r \\ \Phi_i \end{bmatrix} \quad (18)$$

$$\hat{\Phi} = (\mathbf{X}^T \mathbf{X})^{-1} \mathbf{X} \mathbf{h} \quad (19)$$

**Table 4**  
*Hydromechanical Modeling Parameters*

Parameter	Value
<b>Hydraulic properties</b>	
Maximum pumping rate ( $Q_0$ )	$7 \times 10^{-5} \text{ m}^3/\text{s}$
Initial fracture aperture ( $b_0$ )	0.3 mm
Low-permeability host rock porosity ( $\eta_r$ )	0.02 (–)
Low-permeability host rock permeability ( $\kappa_r$ )	$1 \times 10^{-22} \text{ m}^2$
High-permeability host rock porosity ( $\eta_r$ )	0.15 (–)
High-permeability host rock permeability ( $\kappa_r$ )	$3 \times 10^{-15} \text{ m}^2$
<b>Fluid properties</b>	
Fluid density ( $\rho_f$ )	998.2 kg/m <sup>3</sup>
Fluid dynamic viscosity ( $\mu_f$ )	$1.0 \times 10^{-3} \text{ Pa}\cdot\text{s}$
Fluid compressibility ( $\beta_f$ )	$4.8 \times 10^{-10} \text{ Pa}^{-1}$
<b>Prescribed rock elastic moduli</b>	
Young's Modulus ( $E$ )	37.9 GPa
Poisson's ratio ( $\nu$ )	0.1 (–)
<b>Calculated rock elastic moduli</b>	
Host rock bulk modulus ( $K_d$ )	15.7 GPa
Host rock shear modulus ( $G$ )	17.3 GPa

We used this model to explore two scenarios: (a) the isolated effects of fracture hydromechanical behavior and (b) the combined effects of fracture hydromechanics and fracture-host rock fluid exchange on effective fracture hydraulic parameter estimates. We do not consider the effects of pre-existing aperture heterogeneity (absent hydromechanical changes) with this model because the axial symmetry prevents the inclusion of spatially correlated aperture distributions in a geologically realistic manner. In both modeling scenarios, we prescribed elastic moduli (Table 4) consistent with deep bedrock being actively studied as a reservoir for CO<sub>2</sub> injection (Luu et al., 2022).

First, we considered a deformable fracture bounded by low-permeability host rock with permeability and porosity values representative of crystalline or well-cemented sedimentary bedrock (Table 4). The large contrast between fracture permeability ( $\kappa_f = b^2/12$ ) and host rock permeability inhibits fluid leakage from the fracture and concentrates fluid flow along the smooth-walled fracture, allowing us to isolate the fracture hydromechanical behavior and understand its effects on effective fracture parameter estimates.

Next, we loosened the assumption of no fracture-host rock fluid exchange by increasing host rock permeability and porosity values to be consistent with our fracture-host rock fluid exchange modeling analysis (Table 4). The increased host rock permeability allows the host rock to store larger fluid volumes without significantly contributing to flow, providing the opportunity to explore the combined impacts of fracture hydromechanics and fracture-host rock fluid exchange on effective fracture parameter estimates.

## 2.4. Inversion Approach

The numerical models described in Sections 2.1–2.3 provide steady-periodic head phasors for a range of complex hydraulic processes that might occur within a laterally extensive, horizontal fracture during oscillatory hydraulic testing. For this work, we use the head phasors recorded at observation wells as data to obtain the best-fitting fracture hydraulic parameters for each individual oscillatory hydraulic test. Though we do not explicitly work with the amplitude and phase of the recorded head signals, we implicitly invert against them because of the one-to-one relationship between the real and imaginary components of the head phasor and the head signal's amplitude and phase (Patterson & Cardiff, 2023). The numerical inversion approach we describe in this section differs from previously described analytical inversion approaches that relate amplitude attenuation and phase offset to flow parameters (Becker & Gultinan, 2010; Gultinan & Becker, 2015; Renner & Messar, 2006; Saylor et al., 2018), and have been shown to be susceptible to parameter estimates that differ from the true parameter values by more than an order of magnitude (Cardiff & Saylor, 2016).

We applied the numerical gradient-based inversion strategy described by Patterson and Cardiff (2022) to estimate the effective fracture transmissivity ( $T_f$ ) and storativity ( $S_f$ ) that best fit the simulated head phasors. This inversion strategy employs a Levenberg-Marquardt algorithm under a Bayesian framework to find the parameters that minimize the objective function given by:

$$\min_{\mathbf{s}} \frac{1}{2} (\Phi - h(\mathbf{s}))^T \mathbf{R}^{-1} (\Phi - h(\mathbf{s})) \quad (20)$$

where  $\Phi$  is the observed data (i.e., head phasor),  $h(\mathbf{s})$  is the forward model that takes flow parameters as inputs and returns the steady-periodic head phasor, and  $\mathbf{R} = \sigma^2 \mathbf{I}_n$  is the data error covariance matrix, where  $\mathbf{I}_n$  is the identity matrix and  $n$  is the number of phasor coefficients (i.e., data points) used during inversion.

We assumed an uninformative prior distribution—that is, all parameters are equally likely—during inversion. Under this assumption, minimizing the objective function (Equation 20) returns the maximum a posteriori (MAP) model, which is identical to the mean of the posterior distribution (Aster et al., 2018). We employed a non-negativity constraint during inversion by perturbing log-transformed parameters. We declare convergence at the optimal parameters when the relative change in objective function value and the relative change in parameters in consecutive iterations is less than or equal to  $1e-6$ .

Following the analysis approach of previous studies (Gultinan & Becker, 2015; Patterson & Cardiff, 2023; Renner & Messar, 2006; Saylor et al., 2018), we selected a forward model for inversion that inherently assumes the tested fracture can be modeled as a fully confined aquifer of infinite extent with homogeneous and isotropic flow properties (i.e., “stiff, smooth, and solid”). Specifically, we used the analytical model as presented by Rasmussen et al. (2003), which takes fracture hydraulic parameters as inputs and calculates the head phasor as:

$$\Phi = \frac{Q_0}{2\pi T} K_0 \left( r \sqrt{\frac{i\omega}{D}} \right) \quad (21)$$

where  $Q_0 [L^3/T]$  is the peak volumetric flow rate,  $r [L]$  is the radial distance between the pumping and observation well,  $D = T/S [L^2/T]$  is the hydraulic diffusivity, and  $K_0$  is the zero-order modified Bessel function of the second kind.

The chosen forward model (Equation 21) is equivalent to and employs the same assumptions as the Theis solution for drawdown in a fully confined aquifer, with the exception of an oscillatory pumping rate as opposed to constant-rate pumping. More specifically, this forward model assumes a non-deforming, parallel plate fracture of infinite areal extent embedded in an impermeable host rock. It also assumes steady-state hydraulic conditions before testing and no head change at infinite radial distance.

## 3. Modeling Results

In this section, we explore the diagnostic behavior of effective hydraulic parameter estimates obtained via the “stiff, smooth, and solid” assumptions commonly employed to analyze oscillatory hydraulic testing data. Sections 3.1–3.3 describe the period-dependent effective parameter trends for each model (Figures 6d–6l) in detail and explore the effects of multiple interacting mechanisms on effective fracture hydraulic parameter

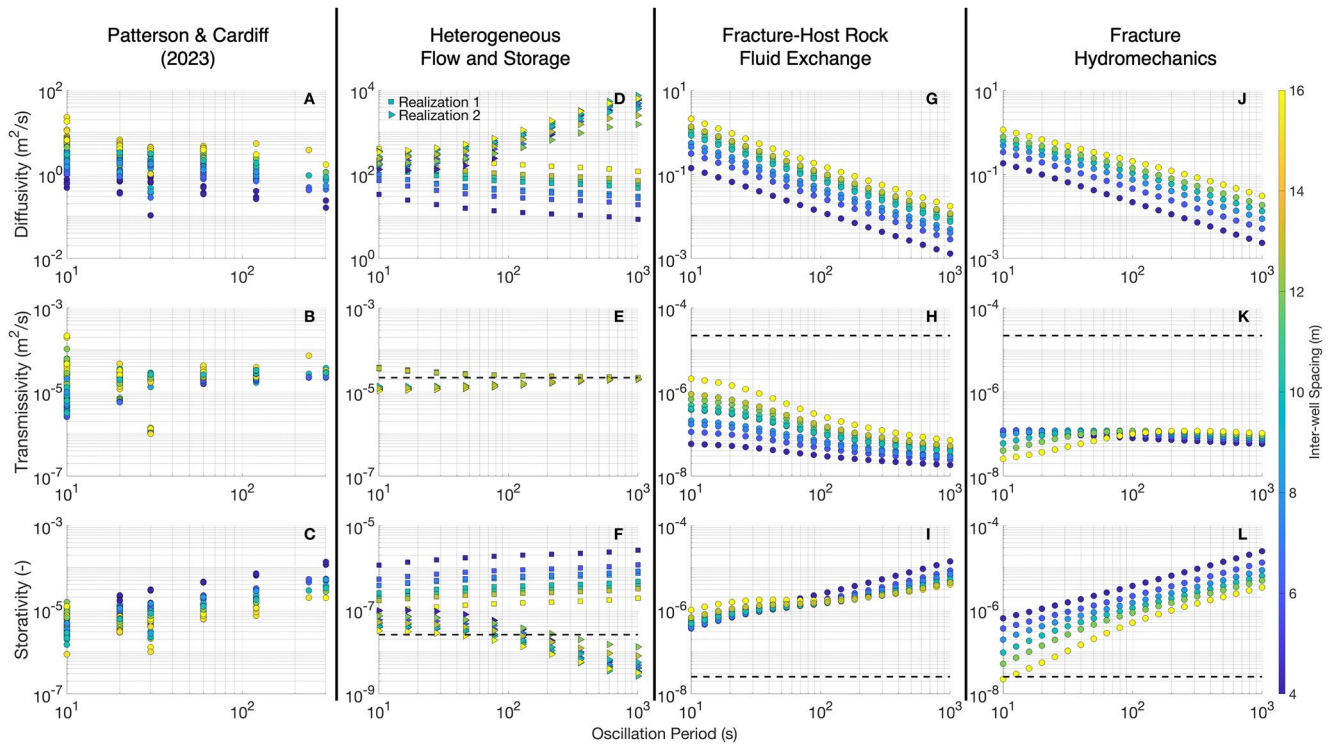


**Figure 6.** Effective fracture hydraulic parameter estimates returned through inverse modeling showing potentially diagnostic period-dependent trends using data generated with the numerical models described in Sections 2.1–2.3. The top row is hydraulic diffusivity, the middle row is transmissivity, and the bottom row is storativity. The first column (a–c) shows available field results reported by Patterson and Cardiff (2023), which serves as a baseline to compare our modeling analysis. The second column shows effective parameter estimates from our heterogeneous flow and storage analysis (d–f), the third column shows effective parameter estimates for the fracture-host rock fluid exchange analysis (g–i), and the last column shows effective parameters for the hydromechanical modeling analysis (j–l). The dashed black lines represent the geometric mean fracture parameter value for each modeling scenario. Plot marker color indicates inter-well spacing, with darker colors representing shorter distances.

estimates. Section 3.4 then demonstrates how these diagnostic responses compare with results (Figures 6a–6c) from recent field fracture characterization experiments presented by Patterson and Cardiff (2023).

### 3.1. Heterogeneous Flow and Storage

The two aperture realizations generated to investigate the effects of heterogeneous flow and storage on effective fracture parameter estimates returned contrasting period-dependent effective fracture hydraulic parameter trends (Figures 6d–6f). When inverting data generated using Realization 1, hydraulic diffusivity estimates decrease by a factor of 3 (Figure 6d), transmissivity estimates decrease by a factor of 2 (Figure 6e)—asymptotically approaching the mean transmissivity value—and storativity estimates increase by a factor of 2 with increasing oscillation period (Figure 6f). As a measure of inversion quality, we calculate a root mean square misfit of  $1.4 \times 10^{-15}$  m between all observed and modeled head phasors for Realization 1.

When inverting data generated using Realization 2, hydraulic diffusivity estimates increase by an order of magnitude (Figure 6d), estimated transmissivity increases by less than a factor of 2—asymptotically approaching the mean transmissivity value (Figure 6e)—and estimated storativity decreases by 1 order of magnitude across the range of tested oscillation periods (Figure 6f), contrasting the period-dependent trends returned with Realization 1. We calculated a root mean square misfit between all observed and modeled head phasors with Realization 2 of  $1.2 \times 10^{-14}$  m. Our modeling analysis also shows spatial trends—consistent across both realizations—in effective hydraulic diffusivity and storativity estimates. Specifically, hydraulic diffusivity increases and estimated storativity decreases with increased inter-well spacings (Figures 6d and 6f).

The contrasting trends in effective fracture flow parameter estimates motivate a stochastic modeling approach to explore the range of period-dependent parameter trends observed across a wide range of randomly generated

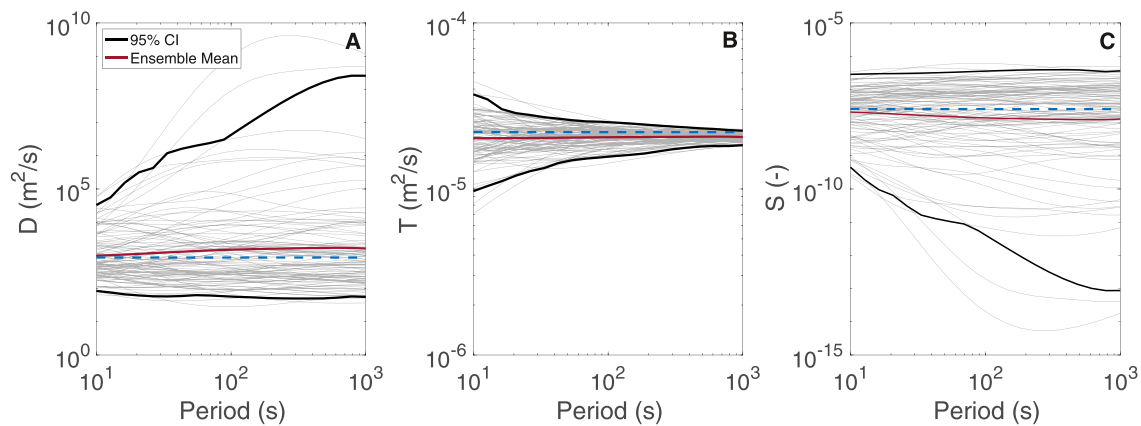


**Figure 7.** Effective hydraulic diffusivity (a), transmissivity (b), and storativity (c) estimates for 100 aperture realizations highlighting the range of period-dependent effective parameter trends across a wide range of heterogeneity geometries. The light gray lines represent individual realizations, the dark black lines represent the ensemble 95% confidence interval, the red line represents the ensemble mean for each fracture parameter, and the dashed blue line represents the prescribed mean for each fracture parameter.

aperture realizations with identical statistical properties. For this stochastic analysis, we used the geostatistical parameters given in Table 2 to generate 100 aperture realizations, simulated oscillatory hydraulic tests at the observation wells for each individual aperture realization, and estimated the effective fracture hydraulic parameters using the inversion approach described in Section 2.4. This stochastic analysis shows examples of increasing, decreasing, and approximately constant effective parameter trends for all hydraulic parameter estimates across the ensemble of aperture realizations, with the ensemble mean parameters closely matching the prescribed mean parameters (Figure 7).

### 3.2. Fracture-Host Rock Fluid Exchange

Inverting data generated in a homogeneous fracture bounded by permeable host rock, our analysis returned period-dependent trends in all estimated hydraulic parameters (Figures 6g–6i). Specifically, hydraulic diffusivity (Figure 6g) and transmissivity estimates (Figure 6h) decrease by approximately 1 order of magnitude and estimated storativity increases by a factor of 5 with increasing oscillation period. Effective storativity estimates increase by a factor of 5 at short and intermediate inter-well spacings (Figure 6i) and remains approximately constant at the longest inter-well spacings (Figure 6i) across the range of tested oscillation periods. The root mean square difference between all modeled and observed phasors is  $6.1 \times 10^{-15}$  m for this modeling scenario.

When inverting data generated with a heterogeneous fracture embedded in a permeable host rock, estimated hydraulic parameters show consistent period-dependence across both aperture realizations (Figure 8), contrasting results that consider only heterogeneous flow and storage (Figures 6d–6f). Hydraulic diffusivity and transmissivity estimates decrease by approximately an order of magnitude (Figures 8a and 8b) and estimated storativity estimates increase with the oscillation period, with the exception of the longest inter-well spacings of Realization 2, which remain approximately constant across the range of tested periods (Figure 8c). These period-dependent trends are consistent with the parameter correlations reported in the homogeneous analysis above (Figures 6g–6i). For the heterogeneous fractures, the root mean square misfit between all modeled and observed phasors is  $1.2 \times 10^{-15}$  m for Realization 1 and  $6.4 \times 10^{-16}$  m for Realization 2.

Inverse modeling results also show spatial trends in effective hydraulic parameter estimates. Specifically, hydraulic diffusivity increases (Figure 8a) and storativity decreases with inter-well spacing (Figure 8c), which is consistent with our heterogeneity inversion results (Figures 6d–6f). In contrast to our aperture heterogeneity analysis, estimated transmissivity increases with inter-well spacing in both the homogeneous fracture (Figures 6g–6i) and heterogeneous fracture modeling scenarios (Figure 8b).

### 3.3. Fracture Hydromechanics

When inverting data generated with a deformable fracture embedded in low-permeability host rock, hydraulic diffusivity estimates decrease by more than an order of magnitude (Figure 6j) estimated transmissivity decreases

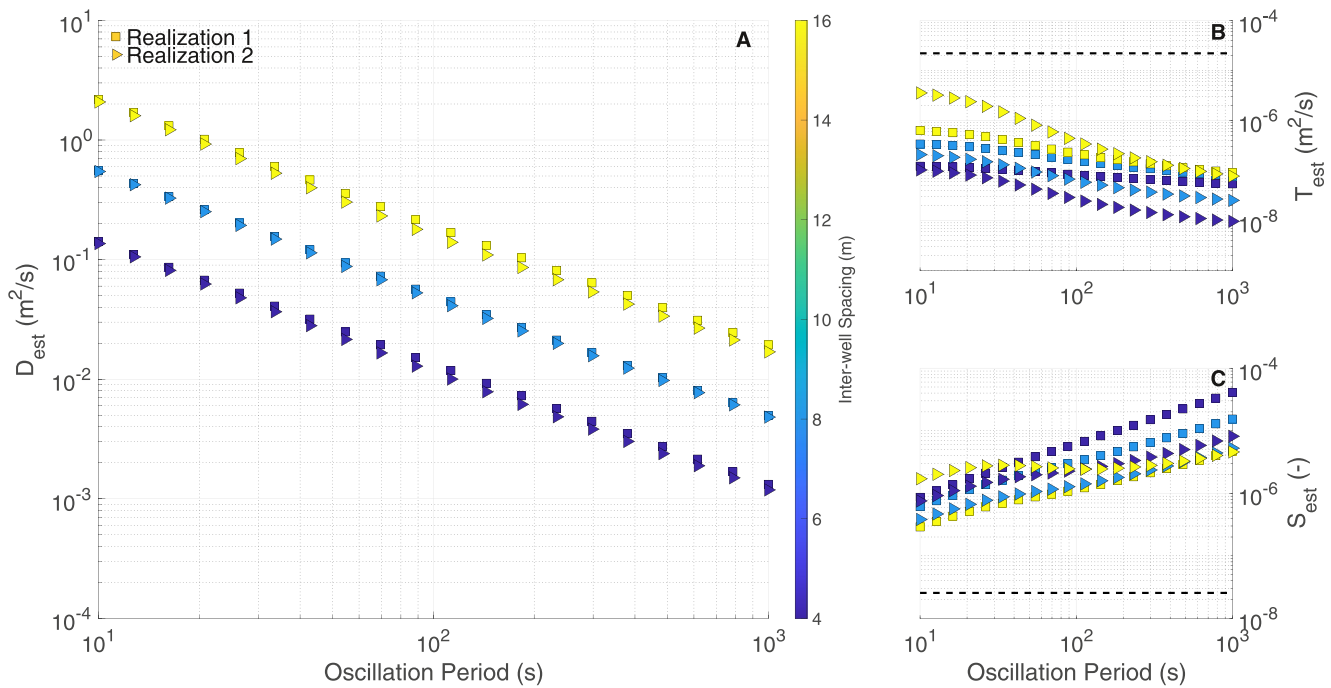


**Figure 8.** Period-dependent hydraulic parameters for a heterogeneous fracture in a permeable host rock. Hydraulic diffusivity (a) and transmissivity (b) estimate decrease with increasing pumping period, while estimated storativity (c) increases with increasing pumping period. The dashed line represents the geometric mean fracture parameter value. Square plot markers represent realization 1 and triangle plot markers indicate realization 2. Plot marker fill color represents inter-well distance, with darker colors indicating shorter distances. For clarity, we show only a subset of modeled inter-well spacings.

by a factor of 2 (Figure 6k), and storativity estimates increase by approximately an order of magnitude across the range of tested oscillation periods (Figure 6l). Hydraulic diffusivity and transmissivity estimates show a positive correlation and storativity shows a negative correlation with inter-well spacing (Figures 6j–6l). The root mean square misfit between all modeled and observed phasors for this scenario is  $6.5 \times 10^{-16}$  m.

Head change and fracture displacement amplitudes decrease across the range of tested oscillation periods a deformable fracture is embedded in a permeable host rock, allowing for fracture-host rock fluid exchange (Figure 9). Specifically, the maximum head amplitude decreases from 0.9 to 0.8 m (Figures 9a and 9c)—an 11% decrease—and the maximum fracture displacement amplitude decreases from 0.4 to 0.3  $\mu\text{m}$  (Figures 9b and 9d), a 25% decrease relative to the low-permeability host rock scenario.

When inverting data generated with a deformable fracture in a permeable host rock, effective storativity and transmissivity estimates (Figure 10), are 10% greater than the low-permeability host rock scenario (Figures 6k and 6l). Parameter estimates returned under this scenario (Figure 10) show identical period-dependent parameter trends and magnitude of change observed in our low-permeability host rock analysis (Figures 6j–6l). Finally, diffusivity and transmissivity estimates increase with inter-well spacing and storativity estimates decrease with inter-well spacing (Figure 10), which is consistent with our low-permeability host rock modeling results (Figures 6j–6l).

### 3.4. Comparison With Available Field Results

Available field results show period-dependent effective hydraulic diffusivity estimates that decrease (Figure 6a) and storativity estimates that increase (Figure 6c) by an order of magnitude across the range of tested oscillation periods. Estimated transmissivity shows large variability that decreases with increasing oscillation period, which gives the appearance of both increasing and decreasing period-dependent trends (Figure 6b). Visual comparison of the period-dependent trends from previous field results with our modeling analyses highlights that fracture hydromechanics (Figures 6j–6l) is the only explored mechanism that consistently reproduces the representative period-dependent trends reported in field experiments (Figures 6a–6c). Our aperture heterogeneity modeling analysis shows effective transmissivity trends that match previous field results; however, hydraulic diffusivity

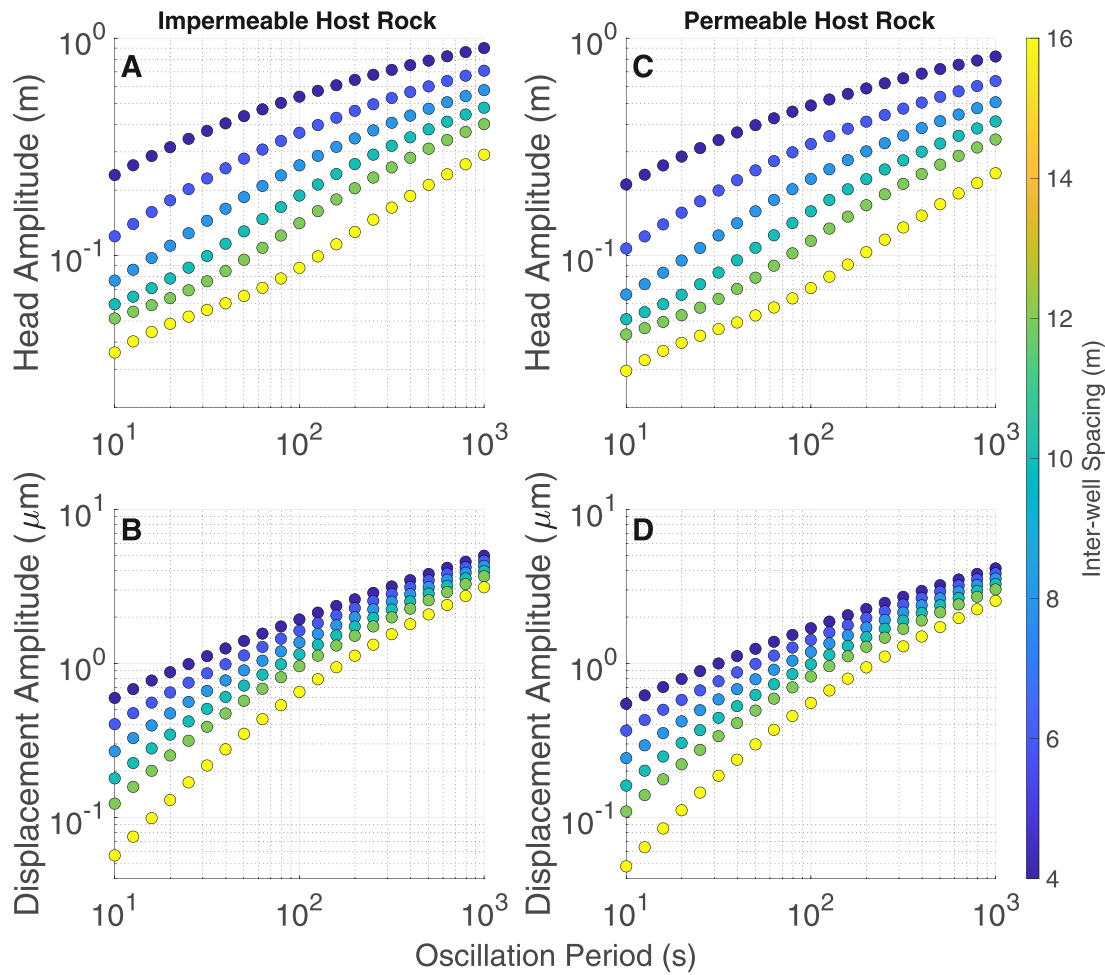


**Figure 9.** Head change (a) and fracture strain (b) amplitude for a deformable fracture in an impermeable host rock across the range of tested oscillation periods. A deformable fracture in a permeable host rock shows lower head change (c) and fracture strain (d) amplitudes across the range of tested oscillation periods. The plot marker color indicates radial distance, with darker colors representing shorter distances.

and storativity trends (Figures 6d and 6g) are not consistent across different aperture realizations or with previous field results (Figures 6a and 6c). Effective parameter estimates from our fracture-host rock fluid exchange show period-dependent hydraulic diffusivity and storativity trends that closely match previous field results; however, transmissivity decreases by more than an order of magnitude (Figure 6h), which is larger than transmissivity trends seen in available field results (Figure 6b).

While a visual comparison of our inverse modeling results with available field results is straightforward (Figure 6), the Pearson correlation coefficient ( $r_p$ ) provides an alternative—and more quantitative—metric to compare the period-dependent trends generated in our numerical modeling experiments to the period-dependent trends from available field results. These correlation coefficients support our visual analysis that fracture hydromechanics is the only explored mechanism that produces parameter correlations of the same direction and magnitude consistent with parameter correlations from previous field results (Table 5).

#### 4. Discussion

Each explored candidate mechanism—heterogeneous flow and storage, fracture-host rock fluid exchange, and fracture hydromechanics—returns period-dependent effective hydraulic parameter estimates when a simple diffusive analytical model is used to determine effective hydraulic parameters, with each modeled process having distinctly different, and potentially diagnostic trends (Figure 6). Though each explored mechanism produces period-dependent trends in effective fracture parameters, fracture hydromechanics (Figures 6j–6l) is the only

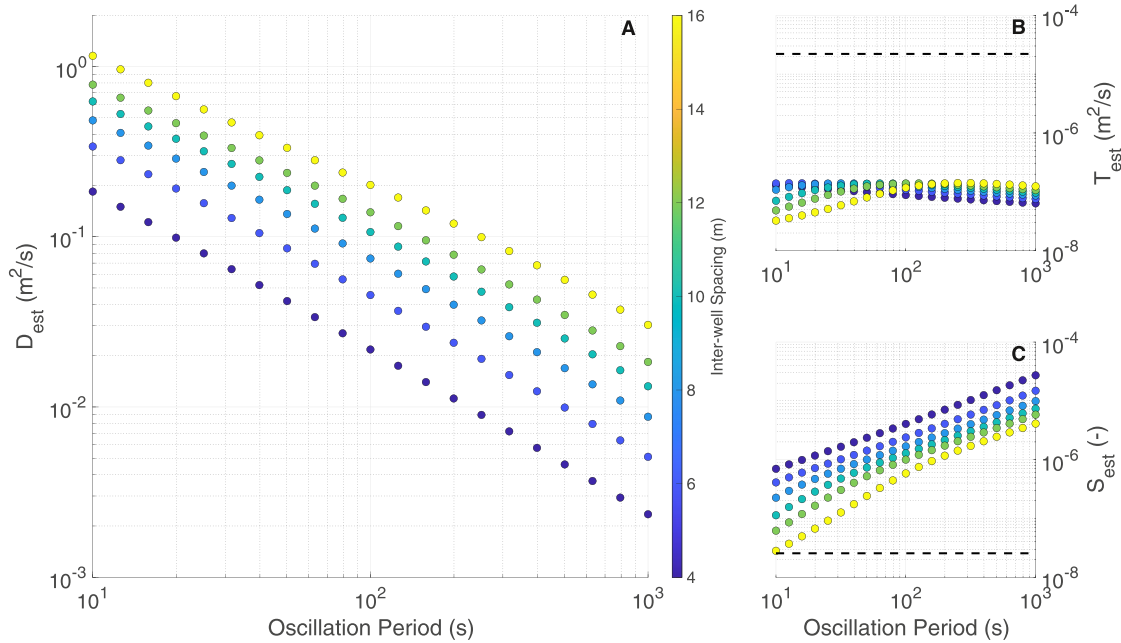


**Figure 10.** Period-dependent effective hydraulic diffusivity (a), transmissivity (b), and storativity (c) estimates for a horizontal, deformable fracture embedded in a permeable host rock. Dashed black lines represent the true fracture transmissivity and storativity values. Plot marker fill color indicates inter-well distance, with darker colors representing shorter distances.

explored mechanism that consistently reproduced the previously reported period-dependent trends (Guiltinan & Becker, 2015; Patterson & Cardiff, 2023; Renner & Messar, 2006; Saylor et al., 2018). We note that our hydromechanical analysis is limited by the fact that we conceptualize a fully open fracture. This modeling choice prevents us from understanding how asperities impact the hydromechanical response and the development of non-linear flows (Cardenas et al., 2007) along the fracture during hydraulic testing—and thus the effective storativity estimates—which represent promising areas for further research.

Fluid storage within deformable fractures during oscillatory hydraulic testing is non-linearly related to pressure changes along the fracture due to the combined effects of fracture normal displacement and fluid compressibility that is variable both in space and time (Murdoch & Germanovich, 2012; Rutqvist et al., 1998; Rutqvist & Stephansson, 2003). Yet, simple diffusive models neglect this hydromechanical coupling and treat storativity as a time-invariant, spatially constant, macroscopic material property of the tested fracture that linearly relates fluid storage to pressure changes. Neglecting the hydromechanical coupling during fractured bedrock characterization leads to overestimated storativity values that increase with increasing oscillation period (Figure 6l), driving a decrease in hydraulic diffusivity estimates with increasing oscillation period (Figure 6j) that is consistent with period-dependent trends reported in the literature (Figures 6a–6c).

Simple diffusive models account for the unmodeled hydromechanical coupling by artificially increasing fracture storativity estimates during inverse modeling, leading to the apparent period-dependence seen in our

**Table 5**  
Pearson Correlation Coefficient ( $r_p$ ) for Parameters Versus Period and Parameters Versus Distance for Each Explored Modeling Scenario

Model type	ln(D) versus ln(period)	ln(T) versus ln(period)	ln(S) versus ln(period)	ln(D) versus ln(distance)	ln(T) versus ln(distance)	ln(S) versus ln(distance)
Field results Patterson and Cardiff (2023)	$r_p = -0.44$	$r_p = 0.34$	$r_p = 0.73$	$r_p = 0.78$	$r_p = 0.25$	$r_p = -0.51$
Heterogenous fracture (Realization 1)	$r_p = -0.45$	$r_p = -0.93$	$r_p = 0.29$	$r_p = 0.88$	$r_p = 0.02$	$r_p = -0.95$
Heterogeneous fracture (Realization 2)	$r_p = 0.92$	$r_p = 0.94$	$r_p = -0.89$	$r_p = 0.11$	$r_p = 0.02$	$r_p = -0.13$
Fracture-host fluid exchange (homogeneous)	$r_p = -0.90$	$r_p = -0.79$	$r_p = 0.89$	$r_p = 0.44$	$r_p = 0.56$	$r_p = -0.14$
Fracture hydromechanics (low-permeability bedrock)	$r_p = -0.85$	$r_p = 0.11$	$r_p = 0.85$	$r_p = 0.52$	$r_p = -0.06$	$r_p = -0.51$

hydromechanical modeling analysis (Figure 6l). We use a simple example to illustrate this point by approximating the fluid storage ( $\Delta V_f$ ) within the fracture out to a distance ( $r$ ) of 4 m using two approaches: (a) we neglect the hydromechanical coupling and approximate the fluid storage using the standard groundwater storage equation (Equation 7) with a fracture storativity of  $2.2 \times 10^{-8}$  (Table 2)—assuming a fully open fracture with a constant initial aperture of 0.3 mm—as follows:

$$\Delta V_f = \pi r^2 S \Delta h \quad (22)$$

and (b) we neglect the effects of fluid compressibility and determine the fluid storage due to fracture displacement alone as follows:

$$\Delta V_f = \pi r^2 \Delta b \quad (23)$$

where  $\Delta V_f$  is the [ $L^3$ ] is the fluid storage,  $\Delta h$  [ $L$ ] is the head change amplitude, and  $\Delta b$  [ $L$ ] is the fracture displacement amplitude. At an oscillation period of 10 s, we simulated a 0.23 m head change amplitude and a fracture displacement amplitude of 0.05  $\mu\text{m}$  at a distance of 4 m from the pumping well (Figure 9), which produces a fluid storage of at least  $2.5 \times 10^{-7} \text{ m}^3$  due to fluid compressibility, and a fluid storage of at least  $2.5 \times 10^{-6} \text{ m}^3$  due to changes in fracture aperture. Now, considering the longest oscillation period of 1,000 s, the recorded head change amplitude was 0.9 m and fracture displacement amplitude was 0.5  $\mu\text{m}$  at a distance of 4 m from the pumping well (Figure 9), which produces a fluid storage of at least  $1.0 \times 10^{-6} \text{ m}^3$  due to fluid compressibility and a fluid storage of at least  $2.5 \times 10^{-5} \text{ m}^3$  due to changes in fracture aperture. This simple calculation shows a consistent 1 order of magnitude increase in fluid storage when the hydromechanical coupling is considered and an increase in fluid storage of almost an order-of-magnitude with increasing oscillation periods. Due to the non-local effects of pressure changes on fracture displacement, this simple approximation is likely an underestimate, but illustrates the relative impact of these two mechanisms on fluid storage within the fracture.

Well geometry with respect to the aperture distribution within a fracture controls the apparent period-dependent trends of effective hydraulic parameters when considering only the effects of heterogeneous flow and storage within the fracture. When the fluid oscillation source is located in a high transmissivity region of the fracture bounded by flow-restricted regions (Figure 2a), longer oscillation periods increase fluid residence time in the fracture. The increased fluid residence time allows fluid diffusion into regions of the fracture that do not significantly contribute to flow (Renner & Messar, 2006)—for example, asperities—leading to increasing storativity and decreasing diffusivity period-dependent trends (Figure 6f). When the fluid oscillation source is located in a flow-restricted region of the fracture (Figure 2c), fluids still concentrate along the high-transmissivity flow backbone; however, longer oscillation periods are required for the fluids to diffuse through the flow-restricted regions and access the high-transmissivity channels causing storativity estimates to decrease and hydraulic diffusivity estimates to increase at longer oscillation periods (Figures 6d–6f). It is important to highlight that this analysis focuses on hydraulic testing conducted in a single fracture. Period-dependent effective parameter estimates produced within complex fracture networks—which likely contains larger degrees of aperture variability and dead-end fractures that do not significantly contribute to flow—remains an open question and area of active investigation.

The hydraulic backbone hypothesis can be conceptualized in a more general sense to say that high-permeability flow channels along the fracture are bounded by low-permeability regions that do not contribute significantly to flow either through dead-end pore space or fluid exchange between the fracture and host rock. This more generalized conceptualization of the backbone hypothesis can be used to explain the positive correlation between storativity and oscillation period seen in our fracture-host rock fluid exchange analysis (Figure 6i). The increased fluid residence time seen with longer oscillation periods allow for increased fluid exchange between the fracture and host rock along pressure gradients, leading to an apparent increase in fracture fluid storage.

The hydromechanical coupling has a minimal effect on transmissivity estimates, with transmissivity showing a factor of 2 decrease across the range of tested periods (Figure 6k), consistent with trends reported by Guiltinan and Becker (2015). Assuming validity of the local cubic law, the largest simulated fracture displacement amplitudes increase fracture transmissivity by only 3%—from  $2.2 \times 10^{-5}$  to  $2.3 \times 10^{-5} \text{ m}^2/\text{s}$ —suggesting effective transmissivity estimates should be approximately constant across the range of tested oscillation periods. Guiltinan and Becker (2015) attribute the period-dependence in effective transmissivity estimates to decreasing pressure amplitudes at the longest oscillation periods leading to decreasing fracture displacement amplitudes during their

oscillatory slug testing experiments. However, our pressure, and thus fracture displacement, amplitudes increase with increasing oscillation period (Figure 9), which should generate a trend of increasing transmissivity if the apparent period-dependence is driven by fracture displacement amplitudes. Therefore, we suggest that the apparent period-dependence in effective transmissivity estimates occurs as a result of larger volumes of the host rock permeability being averaged into the observation signal, and thus effective transmissivity estimates, at longer oscillation periods (Cardiff et al., 2013).

Considering multiple interacting hydraulic processes occurring within a fracture during oscillatory hydraulic testing produces minimal changes in the effective hydraulic parameters returned through inverse modeling (Figure 10), compared to fracture hydromechanics alone (Figures 6j–6l). Though increasing host rock permeability allows for fluid storage within the host rock and aperture heterogeneity can lead to stored fluids within flow-restricted regions of the fracture, the fluid volumes are negligible compared to fluid volume changes associated with fracture normal displacement. While the consideration of combined impacts is critical for accurate predictive simulations of mass and energy transport through fractured bedrock systems, our analysis suggests that fracture hydromechanical behavior is the most critical process to consider when characterizing effective fracture hydraulic properties.

## 5. Conclusions

Increased interest in the use of oscillatory pressure signals to characterize fracture hydraulic parameters has led to unexpected results as these data are analyzed with simple “stiff, smooth, and solid” diffusive models of fracture flow behaviors. Several field experiments conducted in fractured bedrock reported an apparent period-dependence in effective flow parameter estimates—with hydraulic diffusivity and transmissivity showing a negative correlation with oscillation period and storativity estimates showing a positive correlation—indicating the presence of unmodeled hydraulic processes occurring within tested fractures not represented with simple diffusive models. This repeatable apparent period-dependence across multiple field studies and the inability to account for the trends using simple analytical modeling approaches, emphasizes the need for more complex modeling approaches and the numerical modeling experiments presented in this work, which represents the first modeling study that systematically explores multiple complex hydraulic processes—together and alone—occurring within fractures and their impact on effective parameter estimates returned through oscillatory hydraulic testing.

Given the repeatability of these trends and the fact that they are most consistent with our hydromechanical modeling analysis, we conclude that this apparent period-dependence results from the hydromechanical response of the fracture during oscillatory hydraulic testing. Though our hydromechanical modeling analysis reproduces the period-dependent parameter trends reported in the literature, these modeling analyses highlight a range of unrepresented flow processes when applying simple diffusive models to characterize fractured bedrock. Specifically, we demonstrate that fracture heterogeneity, fracture-host rock fluid exchange, and fracture hydromechanics all produce period-dependent flow parameters with distinctly different diagnostic imprints when applying “stiff, smooth, and solid” diffusive models to estimate effective fracture hydraulic parameters. These simple analytical approaches represent a rapid analysis strategy that could provide practitioners with additional information about complex hydraulic processes unrepresented in their initial characterization and help guide more targeted numerical modeling characterization efforts. These results highlight the need to develop more complex numerical models that account for this hydromechanical behavior when characterizing fractured bedrock aquifers.

## Nomenclature

$b$	Fracture aperture (m)
$\Delta b$	Fracture displacement amplitude (m)
$D$	Hydraulic diffusivity ( $\text{m}^2/\text{s}$ )
$E$	Young's Modulus of host rock (Pa)
$G$	Shear modulus of host rock (Pa)
$h$	Hydraulic head (m)
$\Delta h$	Hydraulic head amplitude (m)
$K$	Hydraulic conductivity (m/s)
$K_d$	Drained bulk modulus of rock (Pa)

$\mathbf{n}$	Boundary outward normal vector
$P$	Oscillation period (s)
$p$	Fluid pressure (Pa)
$Q_\omega$	Pumping signal phasor (1/s)
$Q_0$	Peak volumetric flow rate (m <sup>3</sup> /s)
$q_l$	Fluid leak-off from fracture (Pa/s)
$q(t)$	Volumetric flow rate signal (m <sup>3</sup> /s)
$r$	Radial distance (m)
$r_f$	Fracture radius (m)
$r_p$	Pearson correlation coefficient (–)
$S$	Storativity (–)
$\bar{S}$	Mean storativity (–)
$S_s$	Specific storage (1/m)
$T$	Fracture transmissivity (m <sup>2</sup> /s)
$\bar{T}$	Mean fracture transmissivity (m <sup>2</sup> /s)
$t$	Time (s)
$t_s$	Pumping ramp-up time (s)
$t_{off}$	Time offset relative to sine wave (–)
$u$	Displacement of host rock (m)
$\Delta V$	Fluid storage (m <sup>3</sup> )
$v_f$	Fluid velocity (m/s)
$\beta_f$	Fluid compressibility (1/Pa)
$\eta$	Porosity (–)
$\Gamma_d$	Dirichlet boundary condition
$\Gamma_n$	Neumann boundary condition
$\gamma_f$	Fluid specific weight (kg/(m <sup>2</sup> s <sup>2</sup> ))
$\kappa$	Permeability (m <sup>2</sup> )
$\mu_f$	Fluid dynamic viscosity (Pa·s)
$\nu$	Poisson's ratio (–)
$\Omega$	Model domain
$\omega$	Angular frequency (rad/s)
$\Phi$	Hydraulic head phasor (m)
$\rho_f$	Fluid density (kg/m <sup>3</sup> )

### Subscripts:

$f$	Fluid
$f$	Fracture
$r$	Rock

### Data Availability Statement

No new data are presented in this manuscript. The code used to generate the analysis in this work is available at <https://doi.org/10.5281/zenodo.7627265>.

### References

- Aster, R. C., Borchers, B., & Thurber, C. H. (2018). *Parameter estimation and inverse problems*. Elsevier.
- Auradou, H., Drazer, G., Boschan, A., Hulin, J.-P., & Koplík, J. (2006). Flow channeling in a single fracture induced by shear displacement. *The Deep EGS (Enhanced Geothermal System) Project at Soultz-Sous-Forêts, Alsace, France*, 35(5), 576–588. <https://doi.org/10.1016/j.geothermics.2006.11.004>
- Bakhos, T., Cardiff, M., Barrash, W., & Kitanidis, P. K. (2014). Data processing for oscillatory pumping tests. *Journal of Hydrology*, 511, 310–319. <https://doi.org/10.1016/j.jhydrol.2014.01.007>
- Becker, M. W., Ciervo, C., Cole, M., Coleman, T., & Mondanos, M. (2017). Fracture hydromechanical response measured by fiber optic distributed acoustic sensing at milliHertz frequencies. *Geophysical Research Letters*, 44(14), 7295–7302. <https://doi.org/10.1002/2017GL073931>
- Becker, M. W., Coleman, T., & Ciervo, C. (2020). Distributed acoustic sensing as a distributed hydraulic sensor in fractured bedrock. *Water Resources Research*, 56(9), e2020WR028140. <https://doi.org/10.1029/2020WR028140>

### Acknowledgments

The authors thank Drs. Larry Murdoch, Todd Rasmussen, Joërg Renner, and one anonymous reviewer for their constructive comments and detailed feedback, which significantly improved the quality of this work. This work was supported by funding from the National Science Foundation Grant NSF-EAR 1654649 “CAREER: Understanding Transport Processes in Fractured Sedimentary Rock Through Multi-Frequency and Multi-Method Investigations” and through the Wisconsin Department of Natural Resources Contract “Oscillatory Testing and Interpretation at Three Sites in Waushara County” to M. Cardiff.

- Becker, M. W., & Gultinan, E. (2010). Cross-hole periodic hydraulic testing of inter-well connectivity. *Paper presented at the Thirty-fifth Workshop on Geothermal Reservoir Engineering*. Stanford University.
- Becker, M. W., & Tsoulias, G. P. (2010). Comparing flux-averaged and resident concentration in a fractured bedrock using ground penetrating radar. *Water Resources Research*, *46*(9), W09518. <https://doi.org/10.1029/2009wr008260>
- Berre, I., Doster, F., & Keilegavlen, E. (2019). Flow in fractured porous media: A review of conceptual models and discretization approaches. *Transport in Porous Media*, *130*(1), 215–236. <https://doi.org/10.1007/s11242-018-1171-6>
- Black, J. H., & Kipp, K. L. (1981). Determination of hydrogeological parameters using sinusoidal pressure tests: A theoretical appraisal. *Water Resources Research*, *17*(3), 686–692. <https://doi.org/10.1029/WR017i003p00686>
- Bonnet, E., Bour, O., Odling, N. E., Davy, P., Main, I., Cowie, P., & Berkowitz, B. (2001). Scaling of fracture systems in geological media. *Reviews of Geophysics*, *39*(3), 347–383. <https://doi.org/10.1029/1999RG000074>
- Butler, J. J., Jr. (2005). Hydrogeological methods for estimation of spatial variations in hydraulic conductivity. In Y. Rubin & S. Hubbard (Eds.), *Hydrogeophysics* (pp. 23–58). Springer. [https://doi.org/10.1007/1-4020-3102-5\\_2](https://doi.org/10.1007/1-4020-3102-5_2)
- Cappa, F., Guglielmi, Y., Fénart, P., Merrien-Soukatchoff, V., & Thoraval, A. (2005). Hydromechanical interactions in a fractured carbonate reservoir inferred from hydraulic and mechanical measurements. *International Journal of Rock Mechanics and Mining Sciences*, *42*(2), 287–306. <https://doi.org/10.1016/j.ijrmmms.2004.11.006>
- Cappa, F., Guglielmi, Y., Rutqvist, J., Tsang, C.-F., & Thoraval, A. (2006). Hydromechanical modelling of pulse tests that measure fluid pressure and fracture normal displacement at the Coaraze Laboratory site, France. *International Journal of Rock Mechanics and Mining Sciences*, *43*(7), 1062–1082. <https://doi.org/10.1016/j.ijrmmms.2006.03.006>
- Cardenas, M. B., Slotke, D. T., Ketcham, R. A., & Sharp, J. M. (2007). Navier-Stokes flow and transport simulations using real fractures shows heavy tailing due to eddies. *Geophysical Research Letters*, *34*(14), L14404. <https://doi.org/10.1029/2007gl030545>
- Cardiff, M. (2016). OHT3DINV (Version 0.32) [MATLAB]. Retrieved from <https://github.com/wishydro-cardiff/oscillatory-tomography>
- Cardiff, M., Bakhos, T., Kitanidis, P. K., & Barrash, W. (2013). Aquifer heterogeneity characterization with oscillatory pumping: Sensitivity analysis and imaging potential. *Water Resources Research*, *49*(9), 5395–5410. <https://doi.org/10.1002/wrcr.20356>
- Cardiff, M., & Barrash, W. (2015). Analytical and semi-analytical tools for the design of oscillatory pumping tests. *Groundwater*, *53*(6), 896–907. <https://doi.org/10.1111/gwat.12308>
- Cardiff, M., Barrash, W., & Kitanidis, P. K. (2012). A field proof-of-concept of aquifer imaging using 3-D transient hydraulic tomography with modular, temporarily-emplaced equipment. *Water Resources Research*, *48*(5), W05531. <https://doi.org/10.1029/2011WR011704>
- Cardiff, M., & Sayler, C. (2016). Strategies for avoiding errors and ambiguities in the analysis of oscillatory pumping tests. *Journal of Hydrology*, *540*, 1016–1021. <https://doi.org/10.1016/j.jhydrol.2016.06.045>
- Cuss, R. J., Harrington, J. F., Noy, D. J., Sathar, S., & Norris, S. (2015). An experimental study of the flow of gas along synthetic faults of varying orientation to the stress field: Implications for performance assessment of radioactive waste disposal. *Journal of Geophysical Research: Solid Earth*, *120*(5), 3932–3945. <https://doi.org/10.1002/2014JB011333>
- Drazer, G., Auradou, H., Koplik, J., & Hulin, J. P. (2004). Self-affine fronts in self-affine fractures: Large and small-scale structure. *Physical Review Letters*, *92*(1), 014501. <https://doi.org/10.1103/PhysRevLett.92.014501>
- Dutler, N., Valley, B., Gischig, V., Jalali, M., Brixel, B., Krietsch, H., et al. (2020). Hydromechanical insight of fracture opening and closure during in-situ hydraulic fracturing in crystalline rock. *International Journal of Rock Mechanics and Mining Sciences*, *135*, 104450. <https://doi.org/10.1016/j.ijrmmms.2020.104450>
- Ferris, J. G. (1952). Cyclic fluctuations of water level as a basis for determining aquifer transmissibility (U.S. Geological Survey Ground Water Note No. 1) (pp. 1–16). <https://doi.org/10.3133/70133368>
- Fischer, P., Jardani, A., Cardiff, M., Lecoq, N., & Jourde, H. (2018). Hydraulic analysis of harmonic pumping tests in frequency and time domains for identifying the conduits networks in a karstic aquifer. *Journal of Hydrology*, *559*, 1039–1053. <https://doi.org/10.1016/j.jhydrol.2018.03.010>
- Fokker, P. A., Borello, E. S., Viberti, D., Verga, F., & van Wees, J.-D. (2021). Pulse testing for monitoring the thermal front in aquifer thermal energy storage. *Geothermics*, *89*, 101942. <https://doi.org/10.1016/j.geothermics.2020.101942>
- Fu, P., Hao, Y., Walsh, S. D. C., & Carrigan, C. R. (2016). Thermal drawdown-induced flow channeling in fractured geothermal reservoirs. *Rock Mechanics and Rock Engineering*, *49*(3), 1001–1024. <https://doi.org/10.1007/s00603-015-0776-0>
- Fu, P., Settgest, R. R., Hao, Y., Morris, J. P., & Ryerson, F. J. (2017). The influence of hydraulic fracturing on carbon storage performance. *Journal of Geophysical Research: Solid Earth*, *122*(12), 9931–9949. <https://doi.org/10.1002/2017JB014942>
- Gellashch, C. A., Bradbury, K. R., Hart, D. J., & Bahr, J. M. (2013). Characterization of fracture connectivity in a siliciclastic bedrock aquifer near a public supply well (Wisconsin, USA). *Hydrogeology Journal*, *21*(2), 383–399. <https://doi.org/10.1007/s10040-012-0914-7>
- Gellashch, C. A., Wang, H. F., Bradbury, K. R., Bahr, J. M., & Lande, L. L. (2014). Reverse water-level fluctuations associated with fracture connectivity. *Groundwater*, *52*(1), 105–117. <https://doi.org/10.1111/gwat.12040>
- Gultinan, E., & Becker, M. W. (2015). Measuring well hydraulic connectivity in fractured bedrock using periodic slug tests. *Journal of Hydrology*, *521*, 100–107. <https://doi.org/10.1016/j.jhydrol.2014.11.066>
- Hakami, E., & Larsson, E. (1996). Aperture measurements and flow experiments on a single natural fracture. *International Journal of Rock Mechanics and Mining Sciences & Geomechanics Abstracts*, *33*(4), 395–404. [https://doi.org/10.1016/0148-9062\(95\)00070-4](https://doi.org/10.1016/0148-9062(95)00070-4)
- Hollaender, F., Hammond, P. S., & Gringarten, A. C. (2002). Harmonic testing for continuous well and reservoir monitoring. *Paper presented at the SPE Annual Technical Conference and Exhibition*. Society of Petroleum Engineers. <https://doi.org/10.2118/77692-MS>
- Johnson, C. R., Greenkorn, R. A., & Woods, E. G. (1966). Pulse-testing: A new method for describing reservoir flow properties between wells. *Journal of Petroleum Technology*, *18*(12), 1599–1604. <https://doi.org/10.2118/1517-PA>
- Klepikova, M. V., Le Borgne, T., Bour, O., Gallagher, K., Hochreutener, R., & Lavenant, N. (2014). Passive temperature tomography experiments to characterize transmissivity and connectivity of preferential flow paths in fractured media. *Journal of Hydrology*, *512*, 549–562. <https://doi.org/10.1016/j.jhydrol.2014.03.018>
- Kuo, C. H. (1972). Determination of reservoir properties from sinusoidal and multirate flow tests in one or more wells. *Society of Petroleum Engineers Journal*, *12*(6), 499–507. <https://doi.org/10.2118/3632-PA>
- Leven, C., & Barrash, W. (2022). Fiber optic pressure measurements open up new experimental possibilities in hydrogeology. *Groundwater*, *60*(1), 125–136. <https://doi.org/10.1111/gwat.13128>
- Luu, K., Schoenball, M., Oldenburg, C. M., & Rutqvist, J. (2022). Coupled hydromechanical modeling of induced seismicity from CO<sub>2</sub> injection in the Illinois Basin. *Journal of Geophysical Research: Solid Earth*, *127*(5), e2021JB023496. <https://doi.org/10.1029/2021JB023496>
- McClure, M. W., & Horne, R. N. (2014). An investigation of stimulation mechanisms in Enhanced Geothermal Systems. *International Journal of Rock Mechanics and Mining Sciences*, *72*, 242–260. <https://doi.org/10.1016/j.ijrmmms.2014.07.011>
- Murdoch, L. C., & Germanovich, L. N. (2006). Analysis of a deformable fracture in permeable material. *International Journal for Numerical and Analytical Methods in Geomechanics*, *30*(6), 529–561. <https://doi.org/10.1002/nag.492>

- Murdoch, L. C., & Germanovich, L. N. (2012). Storage change in a flat-lying fracture during well tests. *Water Resources Research*, 48(12), W12528. <https://doi.org/10.1029/2011WR011571>
- National Academies of Sciences, Engineering, and Medicine. (2020). *Characterization, modeling, monitoring, and remediation of fractured rock*. The National Academies Press. <https://doi.org/10.17226/21742>
- Neretnieks, I. (2006). Channeling with diffusion into stagnant water and into a matrix in series. *Water Resources Research*, 42(11), W11418. <https://doi.org/10.1029/2005WR004448>
- Patterson, J. R., & Cardiff, M. (2022). Aquifer characterization and uncertainty in multi-frequency oscillatory flow tests: Approach and insights. *Groundwater*, 60(2), 180–191. <https://doi.org/10.1111/gwat.13134>
- Patterson, J. R., & Cardiff, M. (2023). Do simple analytical models capture complex fractured bedrock hydraulics? Oscillatory flow tests suggest not. *Groundwater*, 61(6), 816–833. <https://doi.org/10.1111/gwat.13297>
- Quinn, P. M., Cherry, J. A., & Parker, B. L. (2011). Quantification of non-Darcian flow observed during packer testing in fractured sedimentary rock. *Water Resources Research*, 47(9), W09533. <https://doi.org/10.1029/2010WR009681>
- Rabinovich, A., Barrash, W., Cardiff, M., Hochstetler, D. L., Bakhos, T., Dagan, G., & Kitanidis, P. K. (2015). Frequency dependent hydraulic properties estimated from oscillatory pumping tests in an unconfined aquifer. *Journal of Hydrology*, 531(1), 2–16. <https://doi.org/10.1016/j.jhydrol.2015.08.021>
- Rasmussen, T. C., Haborak, K. G., & Young, M. H. (2003). Estimating aquifer hydraulic properties using sinusoidal pumping at the Savannah River site, South Carolina, USA. *Hydrogeology Journal*, 11(4), 466–482. <https://doi.org/10.1007/s10040-003-0255-7>
- Renner, J., & Messar, M. (2006). Periodic pumping tests. *Geophysical Journal International*, 167(1), 479–493. <https://doi.org/10.1111/j.1365-246X.2006.02984.x>
- Roubinet, D., Linde, N., Jougnot, D., & Irving, J. (2016). Streaming potential modeling in fractured rock: Insights into the identification of hydraulically active fractures. *Geophysical Research Letters*, 43(10), 4937–4944. <https://doi.org/10.1002/2016GL068669>
- Rutqvist, J., Noorishad, J., Tsang, C.-F., & Stephansson, O. (1998). Determination of fracture storativity in hard rocks using high-pressure injection testing. *Water Resources Research*, 34(10), 2551–2560. <https://doi.org/10.1029/98WR01863>
- Rutqvist, J., & Stephansson, O. (2003). The role of hydromechanical coupling in fractured rock engineering. *Hydrogeology Journal*, 11(1), 7–40. <https://doi.org/10.1007/s10040-002-0241-5>
- Salina Borello, E., Fokker, P. A., Viberti, D., Verga, F., Hofmann, H., Meier, P., et al. (2019). Harmonic pulse testing for well monitoring: Application to a fractured geothermal reservoir. *Water Resources Research*, 55(6), 4727–4744. <https://doi.org/10.1029/2018WR024029>
- Saylor, C., Cardiff, M., & Fort, M. D. (2018). Understanding the geometry of connected fracture flow with multiperiod oscillatory hydraulic tests. *Groundwater*, 56(2), 276–287. <https://doi.org/10.1111/gwat.12580>
- Schmidt, P., Dutler, N., & Steeb, H. (2021). Importance of fracture deformation throughout hydraulic testing under in situ conditions. *Geophysical Journal International*, 228(1), 493–509. <https://doi.org/10.1093/gji/ggab354>
- Schweisinger, T., Svenson, E. J., & Murdoch, L. C. (2009). Introduction to hydromechanical well tests in fractured rock aquifers. *Groundwater*, 47(1), 69–79. <https://doi.org/10.1111/j.1745-6584.2008.00501.x>
- Schweisinger, T., Svenson, E. J., & Murdoch, L. C. (2011). Hydromechanical behavior during constant-rate pumping tests in fractured gneiss. *Hydrogeology Journal*, 19(5), 963–980. <https://doi.org/10.1007/s10040-011-0728-z>
- Sobolevskaja, V., Cardenas, M. B., Hasanov, A. K., & Knappett, P. S. K. (2021). Aquifer diffusivity estimation through joint inversion of the amplitude ratios and time lags of dominant frequencies of fluctuating head. *Water Resources Research*, 57(6), e2020WR027912. <https://doi.org/10.1029/2020WR027912>
- Sun, A. Y., Lu, J., & Hovorka, S. (2015). A harmonic pulse testing method for leakage detection in deep subsurface storage formations. *Water Resources Research*, 51(6), 4263–4281. <https://doi.org/10.1002/2014wr016567>
- Sun, Y., & Tong, C. (2017). Dynamic reduced-order models of integrated physics-specific systems for carbon sequestration. *Geomechanics and Geophysics for Geo-Energy and Geo-Resources*, 3(3), 315–325. <https://doi.org/10.1007/s40948-017-0061-7>
- Svenson, E., Schweisinger, T., & Murdoch, L. C. (2007). Analysis of the hydromechanical behavior of a flat-lying fracture during a slug test. *Journal of Hydrology*, 347(1–2), 35–47. <https://doi.org/10.1016/j.jhydrol.2007.08.020>
- Svenson, E., Schweisinger, T., & Murdoch, L. C. (2008). Field evaluation of the hydromechanical behavior of flat-lying fractures during slug tests. *Journal of Hydrology*, 359(1), 30–45. <https://doi.org/10.1016/j.jhydrol.2008.06.004>
- Talley, J., Baker, G. S., Becker, M. W., & Beyrle, N. (2005). Four dimensional mapping of tracer channelization in subhorizontal bedrock fractures using surface ground penetrating radar. *Geophysical Research Letters*, 32(4), L04401. <https://doi.org/10.1029/2004gl021974>
- Tsang, C.-F., Neretnieks, I., & Tsang, Y. (2015). Hydrologic issues associated with nuclear waste repositories. *Water Resources Research*, 51(9), 6923–6972. <https://doi.org/10.1002/2015WR017641>
- Vinci, C., Renner, J., & Steeb, H. (2014). A hybrid-dimensional approach for an efficient numerical modeling of the hydro-mechanics of fractures. *Water Resources Research*, 50(2), 1616–1635. <https://doi.org/10.1002/2013WR014154>
- Vinci, C., Steeb, H., & Renner, J. (2015). The imprint of hydro-mechanics of fractures in periodic pumping tests. *Geophysical Journal International*, 202(3), 1613–1626. <https://doi.org/10.1093/gji/ggv247>
- Wu, H., Fu, P., Morris, J. P., Mattson, E. D., Neupane, G., Smith, M. M., et al. (2021). Characterization of flow and transport in a fracture network at the EGS Collab field experiment through stochastic modeling of tracer recovery. *Journal of Hydrology*, 593, 125888. <https://doi.org/10.1016/j.jhydrol.2020.125888>
- Xing, Y., Liu, Q., Hu, R., Gu, H., Taherdangkoo, R., Yang, H., & Ptak, T. (2022). A general numerical model for water level response to harmonic disturbances in aquifers considering wellbore effects. *Journal of Hydrology*, 609, 127678. <https://doi.org/10.1016/j.jhydrol.2022.127678>
- Zimmerman, R. W., & Bodvarsson, G. S. (1996). Hydraulic conductivity of rock fractures. *Transport in Porous Media*, 23(1), 1–30. <https://doi.org/10.1007/BF00145263>